*The Aeronautical Journal* (2026), 1–26
doi:10.1017/aer.2026.10185

RESEARCH ARTICLE

# Contrail formation: generalised theory and a mitigation proposition for fuel-cell-propelled aircraft

Dennis Hillenbrand[1,2] and Simon Unterstrasser[1]

[1]Deutsches Zentrum für Luft- und Raumfahrt, Institut für Physik der Atmosphäre, Oberpfaffenhofen, Germany
[2]Delft University of Technology, Aerospace Engineering, Section Aircraft Noise and Climate Effects, Delft, the Netherlands
**Corresponding author:** Dennis Hillenbrand; Email: dennis.hillenbrand@dlr.de

**Received:** 2 October 2025 UTC; **Revised:** 30 April 2026 UTC; **Accepted:** 30 April 2026 UTC

**Keywords:** contrail formation; fuel cell; hydrogen; sustainable aviation; thermodynamics

## Abstract

This study presents a generalised theory that describes the thermodynamical processes during mixing of a moist aircraft exhaust with the ambient air and allows one to decide whether or not a contrail forms. Usage of alternative fuels like hydrogen or ammonia increases the moisture content in aircraft plumes compared to current kerosene combustion. Our analysis compares the thermodynamic plume evolution for the classical mixing line and a novel generalised formulation. Additionally, both formulations are used to evaluate the limiting ambient temperature, above which an aircraft does not produce a contrail. We find that the inaccuracies introduced by the classical mixing line cancel each other out, leading to negligible differences between both formulations. Furthermore, the impact of potential heat and water vapour recuperation systems on contrail formation behind fuel-cell-propelled aircraft is investigated. Reducing the exhaust's thermal energy by technical means increases the contrail formation propensity. Especially, if fuels with high hydrogen content are used, plumes with reduced heat content could reach supersaturation values above 500%. This can trigger liquid water droplet formation directly from the gas phase, a process absent in conventional contrail scenarios, and may increase the number of formed ice crystals drastically. A concurrent increase in ice crystal numbers and contrail formation propensity would increase the contrail-cirrus climate impact. To mitigate this scenario, our analysis identifies requirements on the reduction of exhaust water vapour to suppress contrail formation by technical means and reduce the potential contrail climate impact by fuel-cell-propelled aircraft.

## Nomenclature

| | |
|---|---|
| $c_p$ | heat capacity, J kg$^{-1}$ K$^{-1}$ |
| $EI_{H_2O}$ | emission index of water vapour, kg kg$^{-1}$ |
| $F$ | thrust of the aircraft, N |
| $G$ | slope of the mixing line, Pa K$^{-1}$ |
| $G_{FC}$ | slope of the mixing line for fuel cell systems, Pa K$^{-1}$ |
| $h_a$ | ambient enthalpy, J kg$^{-1}$ K$^{-1}$ |
| $h_E$ | exhaust enthalpy, J kg$^{-1}$ K$^{-1}$ |
| $h_{mix}$ | plume enthalpy, J kg$^{-1}$ K$^{-1}$ |
| $m_a$ | mass of ambient air, kg |
| $m_E$ | exhaust mass, kg |
| $m_{mix}$ | plume mass, kg |
| $N$ | dilution factor, 1 |
| $N_E$ | exhaust dilution factor, 1 |
| $p_a$ | ambient pressure, Pa |
| $p_{w,sat}$ | water saturation pressure, Pa |
| $p_{wv,a}$ | ambient water vapour partial pressure, Pa |
| $p_{wv,mix}$ | plume water vapour partial pressure, Pa |

| | |
|---|---|
| $Q$ | lower heating value, J kg$^{-1}$ |
| $Q_{\text{avail}}$ | heat available for contrail formation, J |
| $q_{\text{a}}$ | ambient specific humidity, kg kg$^{-1}$ |
| $q_{\text{E}}$ | exhaust specific humidity, kg kg$^{-1}$ |
| $q_{\text{mix}}$ | plume specific humidity, kg kg$^{-1}$ |
| $\widehat{q}$ | linearised specific humidity, mass mixing ratio, kg kg$^{-1}$ |
| $T_{\text{frz}}$ | homogeneous freezing temperature, K |
| $T_{\text{LM}}$ | temperature at which the mixing line and saturation pressure curve touch, K |
| $T_{\text{mix}}$ | plume temperature, K |
| $\widehat{T}_{\text{lim}}$ | limiting temperature for contrail formation, K |
| $u_{\text{AC}}$ | aircraft velocity, m s$^{-1}$ |

## Greek symbols

| | |
|---|---|
| $\gamma$ | relative emission factor of water vapour, 1 |
| $\delta$ | relative emission factor of heat, 1 |
| $\eta$ | overall propulsion efficiency, 1 |
| $\epsilon$ | ratio of molar masses of water and dry air, 1 |
| $\zeta$ | water vapour-to-heat ratio, kg J$^{-1}$ |
| $\zeta_{\text{norm}}$ | kerosene normalised water vapour-to-heat ratio, 1 |
| $\lambda$ | ratio between relative emission factor of water vapour and heat, 1 |

## Abbreviations

| | |
|---|---|
| $CO_2$ | carbon dioxide |
| DA | dry air |
| FC | fuel cell |
| $H_2$ | hydrogen |
| HDN | homogeneous droplet nucleation |
| ISA | International Standard Atmosphere |
| ISSR | ice super-saturated region |
| LNG | liquid natural gas |
| $NO_x$ | nitrogen oxides |
| PEM | proton exchange membrane |
| $RH_i$ | relative humidity over ice |
| $RH_w$ | relative humidity over water |
| SAC | Schmidt Appleman criterion |
| SAF | sustainable aviation fuels |
| SO | solid oxide |
| WV | water vapour |

## 1.0 Introduction

### *1.1 Motivation*

The aviation industry is estimated to contribute approximately 3.5% to the global anthropogenic effective radiative forcing [1]. Moreover, the growing demand for air travel is expected to increase the number of flights by an average 2.5% per year over Europe until 2030 [2]. Conversely, the European Commission has set ambitious targets for the reduction of $CO_2$ and $NO_x$ emissions by the aviation industry as outlined in its 'Flightpath-2050 report [3]. Meeting these goals despite the expected growth of the aviation industry is challenging, but essential nonetheless.

Notably, $CO_2$ emissions may account for less than half of the total aviation effective radiative forcing, with the remaining share attributed to non-$CO_2$ effects, such as $NO_x$ emissions and contrails [1]. The largest contributors to the total aviation radiative forcing are contrail-cirrus (see Fig. 1 in Ref. [4]).

https://doi.org/10.1017/aer.2026.10185 Published online by Cambridge University Press

Contrail-cirrus spread and persist only in ice super-saturated regions (ISSR), where the ambient relative humidity $RH_{i,a} \gtrapprox 100\%$. The contrail-cirrus radiative impact is more challenging to quantify than the effect of increasing $CO_2$ concentration, which can be approximated by aggregating historical $CO_2$ emissions. These uncertainties arise from the large range of involved spatial scales and the complex interplay between emission quantities and local environmental conditions, which are subject to weather variability [5].

While the major environmental goals of future aircraft technologies are the net reduction of $CO_2$ and $NO_x$ emissions (besides noise and local air quality aspects), it is also crucial to ensure that these technologies do not result in an enhancement of the radiative impact of contrail-cirrus. This would happen if contrails formed more frequently, lived longer, or were optically thicker.

The well-known Schmidt–Appleman criterion (SAC) was first derived by Ref. [6, 7], while Ref. [8] introduced the terminology and presented an improved derivation. It states that a contrail forms when the ambient temperature is below a limiting temperature, which depends on the emission and atmospheric properties. This limiting temperature is around 225K to 230K for conventional kerosene combustion. The limiting temperature is lower when the amount of emitted water vapour (WV) is reduced and/or the amount of emitted heat is increased. These emissions change by switching to alternative fuels for combustion or using electrical propulsion systems like fuel cells (FC). There are several publications dealing with a SAC that is adapted to specific propulsion systems of aircraft. Ref. [9] provides a formulation for an FC-powered aircraft, while Ref. [10] extended the SAC to cover hybrid-electric aircraft. Recently, Ref. [11] analysed contrail formation for a large variety of propulsion systems.

For fuels like pure hydrogen or ammonia, the energy-specific WV emission and the limiting temperature increase, and contrail formation is possible at lower flight altitudes [12]. The increase in potential contrail formation regions compared to current kerosene engines has been shown for hydrogen combustion [13] and hydrogen-based fuel cells [14]. A recent study [15] investigated the influence of future aircraft designs on persistent contrail formation (i.e. formation criterion combined with a persistence criterion), utilising ERA5 data. Their analysis revealed that persistent contrail formation is predominantly constrained by the occurrence of ISSRs, with aircraft design exerting a relatively minor impact. Nevertheless, they conclude that using pure hydrogen will increase the contrail formation propensity compared to current state-of-the-art kerosene combustion.

### *1.2 Future propulsion systems for aircraft*

Proposed future propulsion systems range from using combustion of kerosene-like fuels, such as sustainable aviation fuels (SAFs) to electrical propeller systems. Additionally, hybrid propulsion systems combining combustion and an electrical energy source are currently under investigation [16]. Several SAFs are already in use nowadays as blends with conventional kerosene. SAFs are considered to be an important short/mid-term solution for a more sustainable aviation sector [17]. A review on the influence of using SAFs on contrail formation is given in Ref. [18]. The implementation of pure hydrogen in the aviation sector will need more time than that of SAF, as hydrogen usage increases the complexity of the whole aircraft system e.g. due to storage conditions of hydrogen, which has to be cooled and/or pressurised to remain liquid. Additionally, the volumetric energy density of hydrogen is small, rendering other aircraft designs necessary to be able to store a sufficient amount of hydrogen [19]. Ref. [20] provides an extensive overview of possible future fuels, including organic fuels like SAF, liquid methane and alcohols, and non-organic fuels like pure hydrogen and ammonia. The advantage of using non-organic fuels is that the emitted gas is free of $CO_2$. They conclude that liquid hydrogen is probably the most viable fuel to achieve sustainable aviation in the future. Nevertheless, the transition to a more sustainable aviation industry should involve several fuel types, as no single fuel type can be produced in a sufficient amount in the near future.

The implementation of FC technology in aviation is projected to happen later than that of hydrogen combustion [16]. As FCs produce electrical energy by chemical reactions, $NO_x$ emissions can be avoided completely for fully electric aircraft. This comes at the price of additional complexity of the system due

https://doi.org/10.1017/aer.2026.10185 Published online by Cambridge University Press

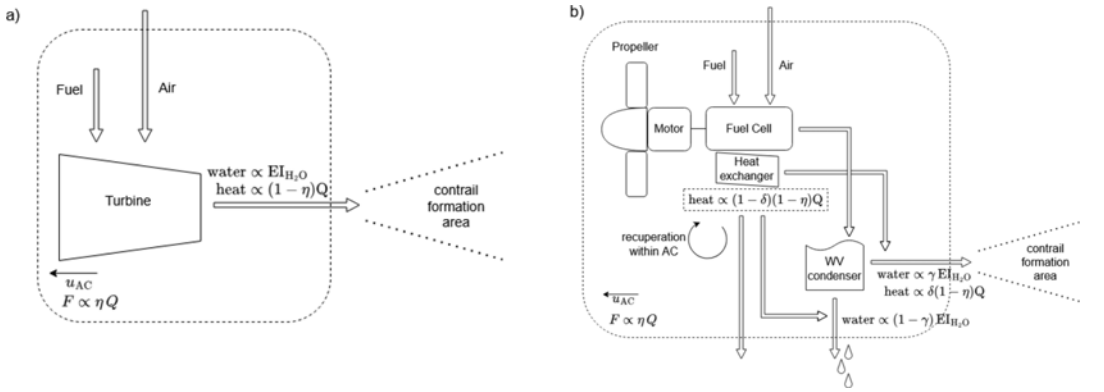


***Figure 1.*** *Schematic representation of contrail-relevant components of aircraft propulsion systems for a conventional gas turbine engine (panel a) and conceptual future FC-based propulsion system with thermal heat management and a WV condenser (panel b).*

*The dashed boundary denotes the aircraft frame moving with the velocity $u_{AC}$, while the dotted lines illustrate the expanding exhaust plume. The arrows depict mass flows. To enhance clarity, all arrows have the same width, yet this does not imply equal magnitude of all mass flow rates.*

to thermal and water management, which are necessary to operate these FCs. Reference [21] investigated several types of FCs and analysed their potential usage in aircraft. According to their analysis, the two most promising FC types are the proton exchange membrane (PEM) and the solid oxide (SO) fuel cell. While the PEM-FC technology is easiest to implement and the most mature technology, SO-FC technology is expected to increase efficiency and reduce the complexity of the system due to higher operating temperatures. For more details on possible future designs of FC-propelled aircraft, refer to e.g. Refs [22–24].

The design of FC-propelled aircraft could also include the possibility to extract both heat and WV before the exhaust is emitted, deliberately or undeliberately altering the exhaust properties. Figure 1 shows a schematic comparison of contrail-relevant components between a conventional gas turbine propulsion system and a hypothetical FC-based propulsion concept. In the FC-based configuration (Fig. 1(b)), the heat exchangers extract thermal energy from the FC stack. This energy is then either utilised within the aircraft systems, released in a separate 'dry-air' exhaust stream or mixed with the 'moist-air' exhaust stream (labelled contrail formation area in the sketch). Additionally, a WV condenser could be included to reduce the amount of WV in the 'moist-air' exhaust stream. The condensed water can then be emitted in a third exhaust stream. The emission factors $\gamma$ and $\delta$ are explained in detail in Section 2.1.

To ensure a sustainable aircraft sector, future propulsion systems and fuels need to reduce both $CO_2$ emissions and non-$CO_2$ effects such as contrail-cirrus, or, at best, avoid them completely. Therefore, several publications have focused on the influence of alternative fuel combustion on contrail properties. Among them are experimental studies providing in-situ measurements of contrail properties [13, 25] behind aircraft flying with SAF. Recently, the first in-situ measurements of a contrail produced by a hydrogen-powered engine have been conducted [26]. Additionally, contrail formation simulations have assessed early contrail properties for hydrogen combustion [27–29]. These studies suggest that the number of formed ice crystals is smaller compared to kerosene combustion due to the reduction of emitted soot particles that serve as condensation nuclei for ice crystals. Recent studies [30, 31] show that for soot-poor or hydrogen combustion plumes, ice crystal formation on oil particles might become important and offset the decrease in ice crystal numbers. As the contrail-cirrus radiative effect decreases with decreasing number of ice crystals [32–34], it is expected that the radiative effect of individual contrails can be reduced by switching from kerosene to pure hydrogen combustion.

https://doi.org/10.1017/aer.2026.10185 Published online by Cambridge University Press

***Table 1.*** *Lower heating value Q [20] and emission index of WV $EI_{H_2O}$ for various fuels*

| Fuel | Kerosene | Hydrogen | Ammonia | LNG |
|---|---|---|---|---|
| Q / MJ $kg^{-1}$ | 43 | 120 | 18.6 | 53.6 |
| $EI_{H_2O}$ / kg $kg^{-1}$ | 1.25 | 8.94 | 1.59 | 2.25 |
| $\zeta$ / kg $MJ^{-1}$ | 0.029 | 0.075 | 0.085 | 0.042 |
| $\zeta_{norm}$ | 1 | 2.57 | 2.95 | 1.45 |

### *1.3 Contrail formation*

The formation of contrails can be assessed using the Schmidt-Appleman criterion [8]. To evaluate the limiting temperature of contrail formation, the mixing process between the initially hot exhaust and the ambient air is described by a mixing line in a WV partial pressure–temperature diagram. While the ambient conditions depend on atmospheric parameters, properties of the initial exhaust plume depend on the propulsion system of the aircraft and fuel used. The slope $G$ of the mixing line is calculated as

$$G = \frac{\mathrm{EI}_{\mathrm{H_2O}}\, c_\mathrm{p}\, p_\mathrm{a}}{Q\,(1-\eta)\,\epsilon} \tag{1}$$

where $EI_{H_2O}$ is the emission index of WV and $Q$ the lower heating value of the utilised fuel, $c_p$ is the heat capacity of air, $p_a$ represents the ambient pressure, $\eta$ is the overall propulsion efficiency and $\epsilon$ is the ratio of the molar masses of water and dry air (DA) $\epsilon = M_{wat}/M_{da} \approx 0.622$. In the remainder, we will refer to the fuel's potential chemical energy that is not used for propulsion as available energy $Q_{avail} = Q\,(1-\eta)$. The thermal and kinetic energy of the exhaust plume contains all or a major fraction of $Q_{avail}$. The SAC assumes that all available energy contributes to the plume thermal energy. Describing $Q\,(1-\eta)$ as available energy $Q_{avail}$ may appear counter-intuitive from an aircraft-propulsion perspective, as $Q_{avail}$ is the waste energy not used for propelling the aircraft. In a contrail-centred viewpoint, this unused energy is the energy that is potentially available within the plume.

Typical values for $EI_{H_2O}$ and $Q$ as well as their ratio $\zeta = EI_{H_2O}/Q$, which appears in the formula for $G$, are given in Table 1 for current and potential future aviation fuels. The normalised factor $\zeta_{norm} = \zeta/\zeta_{kerosene}$ allows for a direct comparison of the effect on the mixing line slope if kerosene is substituted by another fuel. The $\zeta_{norm}$ values show that the WV-to-heat ratio $\zeta$ is small for conventional or synthetic kerosene compared to non-organic fuels, such as pure hydrogen and ammonia. An increase in $G$ leads to higher limiting temperature values of contrail formation, as will be shown later in this section. Notably, the formula for computing the slope $G$ does not account for a dependence on ambient temperature $T_a$ nor on the actual ambient WV partial pressure $p_{wv,a}$, even though the mixing line connects the ambient state $(p_{wv,a}, T_a)$ with the respective plume state. Hence, in the classical theory a change in $T_a$ and/or $p_{wv,a}$ implies only a shift of the mixing line in horizontal and/or vertical direction, but no change of its slope.

The limiting ambient temperature, above which a specified aircraft does not produce a contrail, is denoted as $\widehat{T}_{lim}$. For an (ice) contrail to form, two critical conditions must be met:

1. The ambient temperature $T_a$ is below $\widehat{T}_{lim}$, then the plume becomes supersaturated with respect to water during mixing.
2. The ambient temperature $T_a$ is below $T_{frz}$, the freezing point of supercooled water droplets (possibly including dissolved substances).

Mixing lines for different fuels are depicted in Fig. 2. The solid and dashed grey lines show the saturation pressure of water and ice, respectively. Due to the initially high exhaust temperature, the conditions of the undiluted plume are outside of the plotted range. The prescribed ambient pressure $p_a = 400$ hPa corresponds to flight level FL240, which is representative for regional aircraft. The relative humidity over ice is set as $RH_{i,a} = 100\%$, while the ambient temperature $T_a = 231.4$ K is 10 K lower than defined

https://doi.org/10.1017/aer.2026.10185 Published online by Cambridge University Press

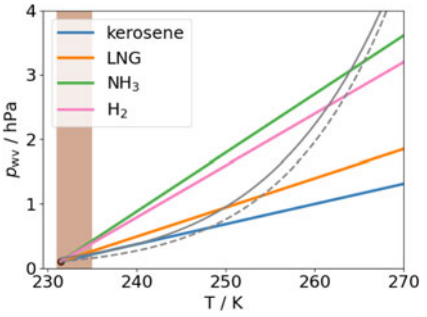


***Figure 2.*** *Mixing lines for fuels given in Tab. 1. The ambient conditions are: $p_a = 400$ hPa, $T_a = 231.4$ K and $RH_{i,a} = 100$ %. The shaded area shows the temperature range below which droplets freeze homogeneously into ice crystals.*

by the International Standard Atmosphere (ISA) at that flight level. The ambient conditions are represented by the black point in the lower left corner in Fig. 2. We assume a constant overall propulsion efficiency of $\eta = 0.4$ for all fuels. For kerosene (blue line), the mixing line touches the liquid water saturation curve but does not cross it. In the displayed example, the ambient temperature was intentionally chosen to be close to $\widehat{T}_{\mathrm{lim}}$ of this scenario. This implies that at higher $T_{\mathrm{a}}$ no contrail would form because the plume will always be sub-saturated with respect to liquid water, while at lower $T_{\mathrm{a}}$ a contrail would form. For liquid natural gas (LNG; orange line), the mixing line is slightly steeper than for kerosene and crosses the liquid water saturation curve, leading to supersaturation of the plume and thus contrail formation. The mixing line slopes for ammonia (green line) and pure hydrogen (pink line) are much larger than for kerosene, leading to high supersaturation values. This analysis already indicates that the contrail formation propensity would be highest when ammonia is used because the largest mixing line slope leads to the highest $\widehat{T}_{\mathrm{lim}}$. Conversely, usage of kerosene leads to the lowest contrail formation propensity of the considered fuels.

The freezing temperature depends on the size and the chemical composition of the water droplets and ranges roughly between 230 K and 235 K for typical plume water droplets [27]. If only condition 1 is fulfilled, a liquid contrail forms that evaporates as the ambient air at cruise conditions is not supersaturated with respect to water. Hence, both conditions are required to form a contrail that consists of ice crystals. Such contrails persist in ice-supersaturated air masses [35, 36], which is a common phenomenon of the upper troposphere [37, 38].

For current kerosene combustion systems, $\widehat{T}_{\mathrm{lim}}$ is typically lower than $T_{\mathrm{frz}}$, rendering the first condition the decisive one for contrail formation. For other fuels, the freezing temperature becomes the crucial condition for contrail formation because $T_{\mathrm{frz}} < \widehat{T}_{\mathrm{lim}}$. For hydrogen combustion, the freezing condition can be the limiting factor in contrail formation [8, 27]. Analogously, $\widehat{T}_{\mathrm{lim}}$ is expected to be the limiting factor for contrail formation when using an FC system using pure hydrogen due to high $\widehat{T}_{\mathrm{lim}}$ values [9, 15].

In this study, the applicability of the mixing line approach of the classical SAC to model the mixing of plumes with high WV-to-heat ratio is re-examined. The derivation of the SAC is based on several linearisations that may not be reasonable for such plumes. A more general relationship between plume temperature and WV content during the mixing process is derived, and this generalised framework is compared to the classical formulation. Furthermore, the impact of potential design options of FC-based aircraft propulsion systems on contrail formation is investigated. We present strategies for manipulating the exhaust properties to suppress or mitigate contrail formation for FC-propelled aircraft.

## 2.0 Generalised contrail formation theory

In this section, relative emission factors are introduced to describe the thermodynamic exhaust conditions of FC-propelled aircraft. Then, a detailed derivation of the classical mixing line theory [8] is presented, which is used to decide whether or not transient supersaturation is reached in the diluting

https://doi.org/10.1017/aer.2026.10185 Published online by Cambridge University Press

plume and a contrail forms. In particular, we explicitly state the underlying assumptions of this approach. Afterwards, a more generally valid theory that does not rely on these assumptions is developed. Instead of a straight mixing line with constant slope $G$, a non-linear relationship between plume temperature and WV partial pressure will be obtained. In analogy to the term 'mixing line', we refer to the new formulation as mixing curve theory.

### *2.1 Relative emission factors*

For aircraft with combustion engines, $Q_{\text{avail}}$ is likely to be fully contained in the exhaust plume as thermal and kinetic energy, even though heat recovery systems might be included in future turbo-fan aircraft to increase the overall propulsion efficiency [39, 40].

In common FC design concepts, however, only a fraction of the generated WV and energy is contained in the moist-air exhaust stream. To account for the potential reduction of emitted WV and heat in FC-propelled aircraft (cf. Fig. 1(b)), we introduce two relative emission factors. While

$$\gamma = \mathrm{EI}_{\mathrm{H_2O,emit}}/\mathrm{EI}_{\mathrm{H_2O}} \tag{2}$$

represents the actual amount of WV emitted compared to the unaltered amount,

$$\delta = Q_{\text{emit}}/Q_{\text{avail}} \tag{3}$$

represents the actual amount of heat emitted compared to its unaltered amount. In future FC systems, $\gamma$ and $\delta$ might be well below 1 for several reasons. First of all, the exhaust and propulsive streams are spatially separated. Hence, the kinetic energy of the propulsive streams and associated friction losses at the propellers reduce the energy content of exhaust plumes. Moreover, Fig. 1(b) indicates the diversion of heat (via heat exchangers) and WV (via WV condenser devices) from the exhaust gas. The diverted heat can be exploited for secondary applications within the aircraft, such as cabin heating, or released in a separate 'dry-air' exhaust stream. Provided that the two exhaust streams are emitted at different locations and do not mix during plume dilution, the energy content of the moist-air exhaust remains reduced. Similarly, the condensed WV might be released as liquid droplets far away from the moist-air exhaust, such that its WV content remains reduced. As contrail formation can only occur inside the diluting 'moist-air' exhaust, we will simply refer to it as 'exhaust' in the remainder of this paper.

The adapted slope for the mixing line of FC systems, taking the relative heat and WV emission factors $\gamma$ and $\delta$ into account, reads

$$G_{\mathrm{FC}} = \frac{\gamma\, \mathrm{EI}_{\mathrm{H_2O}}\, c_{\mathrm{p}}\, p_{\mathrm{a}}}{\delta\, Q\, (1-\eta)\, \epsilon} \tag{4}$$

If all available energy is used to heat the plume and all WV is contained in the exhaust, theoretically $\gamma = \delta = 1$ and the mixing line slope of the FC system is equal to the respective combustion propulsion system. We will discuss the effects of potential WV and heat recuperation systems on contrail formation in detail in Section 4.

### *2.2 Classical derivation of mixing line*

First, we provide an overview of the derivation for the mixing line as presented in Ref. [8]. As the plume dilutes, ambient air is added continuously to the exhaust. Isobaric mixing of the two air parcels is assumed, as the plume pressure relaxes quickly to ambient pressure. One air parcel represents the homogeneous exhaust plume, and the other parcel represents the infinite reservoir of surrounding atmospheric air. In this purely thermodynamic formulation, the effects of microphysical processes are disregarded. For consistency with the original derivation, which was developed for combustion propulsion systems, the relative emission factors are set to $\gamma = \delta = 1$.

https://doi.org/10.1017/aer.2026.10185 Published online by Cambridge University Press

We determine the specific humidity, which is the ratio of the WV mass to the total air mass, and the enthalpy of the mixed plume. The plume's specific humidity can be expressed by

$$\Delta\widehat{q} = \frac{\mathrm{EI}_{\mathrm{H_2O}} - \widehat{q}_{\mathrm{a}}}{N} \approx \frac{\mathrm{EI}_{\mathrm{H_2O}}}{N} \tag{5}$$

where $N$ represents the dilution, which is the air-to-fuel mass ratio of the diluting plume. The ambient specific humidity $\widehat{q}_{\mathrm{a}}$ is negligible compared to the exhaust's specific humidity and is therefore set to zero.

The enthalpy of the plume is treated analogously:

$$\Delta h = \frac{Q\,(1-\eta) - h_{\mathrm{a}}}{N} \approx \frac{Q\,(1-\eta)}{N} \tag{6}$$

Compared to the exhaust enthalpy, the enthalpy value $h_{\mathrm{a}}$ of the ambient air is small and therefore neglected. The excess enthalpy $\Delta h$ can then be used to calculate the excess temperature for each plume condition during mixing

$$\Delta h = \int_{T_a}^{T} c_p \,\mathrm{dT} \approx \bar{c}_p (T - T_a) = \bar{c}_p \Delta T \tag{7}$$

where $\bar{c}_p \approx 1004\ \mathrm{J(kg\ K)}^{-1}$ is chosen as a constant whose value is close to the one of DA at ambient conditions. Equation (7) assumes that the plume kinetic energy contributes negligibly to the plume enthalpy (which is reasonable at least when the plume becomes supersaturated). By combining Equations (5)–(7), $N$ can be eliminated and the change of the plume specific humidity with plume temperature can be expressed as

$$\frac{\Delta\widehat{q}}{\Delta T} = \frac{\mathrm{EI}_{\mathrm{H_2O}} \bar{c}_{\mathrm{p}}}{Q\,(1-\eta)} \tag{8}$$

Following the usual assumption in meteorology, the WV partial pressure is expressed as

$$\widehat{q} = \epsilon\, \frac{p_{\mathrm{wv}}}{p_{\mathrm{a}}} \tag{9}$$

Reformulating $\Delta\widehat{q} = \widehat{q} - \widehat{q}_{\mathrm{a}}$ and $\Delta T = T - T_{\mathrm{a}}$ in Equation (8), using Equation (9) and rearranging gives a linear relation between the WV plume partial pressure and the plume temperature using $G$ from Equation (1):

$$p_{\mathrm{wv}} = p_{\mathrm{wv,a}} + G\,(T - T_{\mathrm{a}}) \tag{10}$$

It is advantageous for the following analysis to describe the plume moisture and thermal energy in terms of partial pressure and plume temperature. Unlike the saturation specific humidity, which depends on the ambient pressure, the WV saturation pressure $p_{\mathrm{w,sat}}$ depends only on temperature. This allows us to compute the limiting temperature $\widehat{T}_{\mathrm{lim}}$ for a given ambient relative humidity by requiring that the slope of the mixing line matches the slope of $p_{\mathrm{w,sat}}$. For this, we introduce the temperature $T_{\mathrm{LM}}$ at which both curves touch each other, implicitly given by:

$$\frac{\mathrm{d}p_{\mathrm{w,\,sat}}(T_{\mathrm{LM}})}{\mathrm{d}T} = G \tag{11}$$

An approximation for the evaluation of $T_{\mathrm{LM}}$ depending on $G$ is given in the appendix of Refs [8] or [9]. The actual limiting temperature $\widehat{T}_{\mathrm{lim}}$ depends on the ambient relative humidity $\mathrm{RH_{w,a}}$ and can be found by solving the following equation:

$$p_{\mathrm{w,sat}}(T_{\mathrm{LM}}) + G\left(\widehat{T}_{\mathrm{lim}} - T_{\mathrm{LM}}\right) = \mathrm{RH_{w,a}}\, p_{\mathrm{w,sat}}\left(\widehat{T}_{\mathrm{lim}}\right) \tag{12}$$

In general, this is an implicit equation that can be solved for $\widehat{T}_{\mathrm{lim}}$ by a Newton iteration. A contrail forms, if the ambient temperature is both lower than $\widehat{T}_{\mathrm{lim}}$ (i.e. the SAC criterion is fulfilled) and $T_{\mathrm{frz}}$ of the water droplets. For ambient temperatures larger than $\widehat{T}_{\mathrm{lim}}$, no contrail forms because the cooling plume remains sub-saturated during the whole mixing process.

https://doi.org/10.1017/aer.2026.10185 Published online by Cambridge University Press

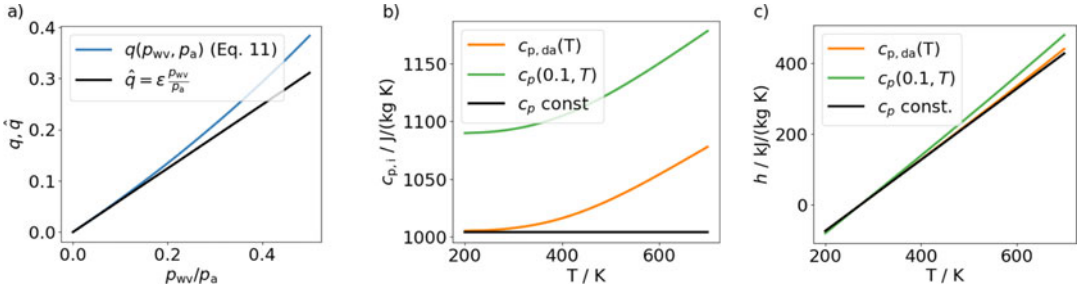


***Figure 3.*** *Exemplary simplifications for the mixing line theory. Black lines show the values used in classical derivation. a) Dependence of specific humidity on the normalised WV partial pressure. b) Dependence of heat capacities on temperature. c) Dependence of enthalpy on temperature.*

### *2.3 Review of assumptions in the classical formulation*

In the past, the classical mixing line has been applied to scenarios of kerosene and hydrogen combustion. However, this formulation may not be applicable to the exhaust plumes generated by FC-propelled aircraft equipped with heat recuperation systems, which can produce moist and relatively cool plumes. Consequently, some assumptions underlying the mixing line derivation (Section 2.2) require re-evaluation.

The first approximation that may not be sufficiently accurate for moist plumes is the linear relation between the specific humidity $q$ and the WV partial pressure $p_{wv}$, given by Equation (9). For this relation, which is used in traditional meteorological formulations, it is assumed that the WV mass within an air parcel is significantly smaller than the DA mass. Consequently, the contribution of $p_{wv}$ to the total pressure is typically neglected, allowing the total pressure to be approximated as the DA pressure $p_{tot} = p_{da}$. For very moist air parcels, this assumption is no longer valid; the pressure of the moist air $p_{tot}$ has to be described as the sum of the WV and DA partial pressures. Hence, the relationship needs to be extended to include the influence of WV on the properties of the moist air parcel:

$$q := \frac{m_{wv}}{m_{tot}} = \frac{\rho_{wv}}{\rho_{tot}} = \frac{\rho_{wv}}{\rho_{da} + \rho_{wv}} = \frac{p_{wv}/R_{wv}}{p_{da}/R_{da} + p_{wv}/R_{wv}} = \frac{\epsilon\, p_{wv}}{p_{da} + \epsilon p_{wv}} = \frac{\epsilon\, p_{wv}}{p_a + (\epsilon - 1) p_{wv}} \tag{13}$$

$m$ denotes the mass, $\rho$ the density and $R_{wv}, R_{da}$ the specific gas constants for WV and DA, respectively. Due to the isobaricity assumption, the total pressure of any air parcel considered equals $p_a$. The discrepancy between this formula and the simplified relation (Equation (9)) is illustrated in Fig. 3(a) and evaluated as a function of the ratio $p_{wv}/p_a$. The simplified formula provides a good approximation for $p_{wv}/p_a < 0.1$, which encompasses the majority of applications in atmospheric science. However, for larger relative WV contents, the two lines diverge, indicating that the simplified formula becomes less accurate the moister the plume is.

The second assumption to be re-evaluated is the use of a constant heat capacity $c_{p,da}$ throughout the entire temperature range of the mixing process. To improve accuracy, it is more appropriate to employ a framework that accounts for the changes in heat capacity as a function of temperature and water content. Consequently, the enthalpy of the plume must be evaluated at each mixing state using the integral expression:

$$h(T) = \int_{T_{ref}}^{T} c_p(q(\tilde{T}), \tilde{T})\, \mathrm{d}\tilde{T} \tag{14}$$

where $T_{ref}$ is a reference temperature at which the enthalpy is set to zero. The heat capacity of moist air is a linear interpolation between the heat capacities $c_{p,wv}(T)$ and $c_{p,da}(T)$ via the specific humidity $q$:

$$c_p(q, T) = q\, c_{p,wv}(T) + (1 - q)\, c_{p,da}(T) \tag{15}$$

https://doi.org/10.1017/aer.2026.10185 Published online by Cambridge University Press

To accurately represent the WV and DA heat capacities, we utilise the parametrisation provided by Ref. [41]. For DA, a composition of 21% oxygen and 79% nitrogen is considered. Reference (41) also gives a parametrisation of the enthalpy that is consistent with their WV and DA heat capacity parametrisation. We employ this parametrisation to calculate the enthalpy of the diluting plume analogously to the heat capacity:

$$h(q, T) = q\, h_{\mathrm{wv}}(T) + (1 - q)\, h_{\mathrm{da}}(T) \tag{16}$$

Figure 3(b) and (c) show the temperature dependence of the heat capacity and enthalpy of moist air, respectively. Both plots compare the value used in the classical derivation (black line) with the temperature-dependent values for DA and for moist air with fixed $q = 0.1$. Even though the differences in the heat capacity diagram are exaggerated for the chosen y-axis range, the relative error between the constant and parametrised heat capacity for moist air exceeds 15% for high temperature values, rendering the usage of a constant heat capacity questionable. The maximum difference for the enthalpy of the moist air is approximately 12%, although it has to be noted that the relative difference depends on the chosen reference value for the enthalpy, which is 273.15 K in the utilised parametrisation.

Moreover, the classical theory drops the ambient terms from Equations (5) and (6) leading to a slope of the mixing line in $\widehat{q}$–$T$ space that is independent of ambient conditions. We deem the errors by this simplification negligible. Nevertheless, the ambient terms are retained in our derivation, as dropping the terms would not simplify the following derivations.

### *2.4 Generalised contrail formation criterion*

In the following, we derive a formulation for the mixing process without the assumptions used in the classical formulation. We start from fundamental physical principles, specifically the conservation laws of mass and energy. As in Section 2.2, isobaric mixing of the plume and ambient air and a homogeneous plume described by a mean plume state is assumed. Note that this implies that the exhaust is instantaneously mixed, which may not be appropriate for modern turbo-fan engines with high bypass ratios. This effect on the mixing line has already been studied in Ref. [42]. In contrast to the classical mixing line, we allow the specific heat capacity and enthalpy to be functions of both temperature and specific humidity. Our objective is to determine the plume specific humidity $q_{\mathrm{mix}}$ and its corresponding temperature $T_{\mathrm{mix}}$ during the mixing process. To this end, the conservation laws governing the total mass, the WV mass and thermal energy of the plume are applied, respectively:

$$\text{total mass conservation} \quad m_{\mathrm{E}} + m_{\mathrm{a}}(t) = m_{\mathrm{mix}}(t) \tag{17}$$

$$\text{water mass conservation} \quad q_{\mathrm{E}}\, m_{\mathrm{E}} + q_{\mathrm{a}}\, m_{\mathrm{a}}(t) = q_{\mathrm{mix}}(t)\, m_{\mathrm{mix}}(t) \tag{18}$$

$$\text{energy conservation} \quad m_{\mathrm{E}}\, h_{\mathrm{E}} + m_{\mathrm{a}}(t)\, h_{\mathrm{a}} = m_{\mathrm{mix}}(t)\, h_{\mathrm{mix}}(t) \tag{19}$$

The indices ‘E’ and ‘a’ correspond to the exhaust and ambient values, respectively. Note that $m_{\mathrm{a}}(t)$ does not describe the (infinite) mass reservoir of ambient air, but the increasing mass already entrained into the plume. In contrast, all other ambient variables correspond to time-constant properties of the ambient atmosphere. The three Equations (17)–(19) are used to calculate the three unknowns of the plume $m_{\mathrm{mix}}, q_{\mathrm{mix}}, h_{\mathrm{mix}}$. Using Equation (13), the specific humidity can be replaced by a function of partial pressure $p_{\mathrm{wv}}$, while the temperature can be calculated from inverting the enthalpy parametrisation of moist air (see Equation (16)) with an iterative solution method. Following these steps yields a relationship with a form similar to the classical mixing line Equation (10).

To calculate the temporal evolution of the specific humidity $q_{\mathrm{mix}}(t)$, we use the temporal derivative of Equation (18), which results in the differential equation

$$\frac{\mathrm{d}q_{\mathrm{mix}}}{\mathrm{d}t} = \frac{\dot{m}_{\mathrm{mix}}}{m_{\mathrm{mix}}}\,(q_{\mathrm{a}} - q_{\mathrm{mix}}) \tag{20}$$

https://doi.org/10.1017/aer.2026.10185 Published online by Cambridge University Press

Accordingly, Equation (19) results in a differential equation for the enthalpy:

$$\frac{\mathrm{d}h_{\mathrm{mix}}}{\mathrm{d}t} = \frac{\dot{m}_{\mathrm{mix}}}{m_{\mathrm{mix}}} \left(h_{\mathrm{a}} - h_{\mathrm{mix}}\right) \tag{21}$$

Now, the combination of Equation (20) and Equation (21) leads to

$$\frac{\mathrm{d}q_{\mathrm{mix}}}{\mathrm{d}h_{\mathrm{mix}}} = \frac{q_{\mathrm{mix}} - q_{\mathrm{a}}}{h_{\mathrm{mix}} - h_{\mathrm{a}}} \tag{22}$$

This simple differential equation results in a linear function between the enthalpy and the specific humidity of the plume. With the initial condition that the mixing line should meet the exhaust condition $q(h_{\mathrm{E}}) = q_{\mathrm{E}}$ the linear specific humidity-enthalpy relation during the mixing process can be expressed as

$$q_{\mathrm{mix}} = q_{\mathrm{a}} + (q_{\mathrm{E}} - q_{\mathrm{a}}) \frac{h_{\mathrm{mix}} - h_{\mathrm{a}}}{h_{\mathrm{E}} - h_{\mathrm{a}}} \tag{23}$$

This relation governs the whole mixing process in a generalised way. If we assumed linear functions $p_{\mathrm{wv,mix}}\,(q_{\mathrm{mix}})$ and $h_{\mathrm{mix}}(T_{\mathrm{mix}})$ (see Equations (7) and (9)), the classical mixing line (Equation (10)) would follow. With the full non-linear relations, we obtain the following implicit relationship between $p_{\mathrm{wv,mix}}$ and $T_{\mathrm{mix}}$:

$$q_{\mathrm{mix}} \left( \frac{1}{q_{\mathrm{E}} - q_{\mathrm{a}}} - \frac{h_{\mathrm{wv}}(T_{\mathrm{mix}}) - h_{\mathrm{da}}(T_{\mathrm{mix}})}{h_{\mathrm{E}} - h_{\mathrm{a}}} \right) = \frac{q_{\mathrm{a}}}{q_{\mathrm{E}} - q_{\mathrm{a}}} + \frac{h_{\mathrm{da}}(T_{\mathrm{mix}}) - h_{\mathrm{a}}}{h_{\mathrm{E}} - h_{\mathrm{a}}} \tag{24}$$

$$\text{with } q_{\mathrm{i}} = \frac{\epsilon\, p_{\mathrm{wv,i}}}{p_{\mathrm{a}} + (\epsilon - 1) p_{\mathrm{wv,i}}} \text{ for i} \in \{\mathrm{mix, E, a}\}$$

In contrast to the classical mixing line, Equation (24) does not explicitly contain fuel properties and the overall propulsion efficiency $\eta$. To obtain a classical formulation of the mixing curve, these parameters can be calculated from the exit conditions

$$q_{\mathrm{E}} = \gamma\, N_{\mathrm{E}}\, \mathrm{EI}_{\mathrm{H_2O}} \tag{25}$$

$$h_{\mathrm{E}} = \delta\, N_{\mathrm{E}}\, Q(1 - \eta), \tag{26}$$

where $N_{\mathrm{E}}$ is the dilution of the exhaust at the exit.
Using a parametrisation for $h_{\mathrm{wv}}$ and $h_{\mathrm{da}}$, e.g. Ref. [41], this equation can be solved for $p_{\mathrm{wv,mix}}$ under specified ambient and initial conditions. The form and behaviour of the generalised mixing curve when changing the input parameters are less apparent than for the classical mixing line. Investigating the effects of fuel properties and ambient conditions on contrail formation is much more straightforward for the classical mixing line, because these are explicitly represented in Equation (10).

The calculation of $\widehat{T}_{\mathrm{lim}}$ is straightforward with the classical mixing line theory. In particular, the independence of $G$ from the ambient state simplifies the determination of $\widehat{T}_{\mathrm{lim}}$. The mixing curve (Equation (24)), however, depends implicitly on the ambient temperature, making it impossible to evaluate the limiting temperature condition (Equation (11)) explicitly. Therefore, we propose a numerical, iterative search for the maximum ambient temperature, at which the relative humidity with respect to water $\mathrm{RH_w}$ is at least 100% during mixing. This ambient temperature is then considered the limiting temperature:

$$\widehat{T}_{\mathrm{lim}} = \max\,(T_{\mathrm{a}}) \;\; | \, \mathrm{RH_{w,max}} \geq 100\% \text{ for Equation (24)} \tag{27}$$

While the solution of this formulation is computationally more demanding than the application of the classical theory, it provides a more generally valid representation of plume mixing with the ambient air.

Microphysical processes play an important role for the plume conditions once the plume becomes supersaturated with respect to water. While the thermodynamic formulation is well-suited to determine whether or not a contrail forms, it does not provide any information on the contrail's properties. To include microphysical processes, the plume mixing has to be resolved in time, which is not necessary for the thermodynamical formulation. The current study focuses on the thermodynamical formulation,

https://doi.org/10.1017/aer.2026.10185 Published online by Cambridge University Press

***Table 2.*** *Parameter settings for different applications for possible future aircraft propulsion systems*

| Name | Fuel | $N_E$ | $\eta$ | $\gamma$ | $\delta$ | $p_a$ / hPa | $T_a$ / K |
|---|---|---|---|---|---|---|---|
| Kero | kerosene | 70 | 0.4 | 1 | 1 | 400 | 230 |
| LNG | methane | 87 | 0.4 | 1 | 1 | 400 | 230 |
| ammo | ammonia | 30 | 0.4 | 1 | 1 | 400 | 230 |
| $H_2C$ | hydrogen | 195 | 0.4 | 1 | 1 | 400 | 230 |
| $H_2FC$ 1 | hydrogen | 195 | 0.4 | 1 | 0.25 | 400 | 230 |
| $H_2FC$ 2 | hydrogen | 195 | 0.4 | 0.25 | 1 | 400 | 230 |
| $H_2FC$ 3 | hydrogen | 195 | 0.4 | 1 | 0.25 | 400 | 210 |
| $H_2FC$ 4 | hydrogen | 195 | 0.4 | 1 | 0.25 | 280 | 230 |

but Appendix A.1 provides a method to include the generalised equations in a numerical microphysical model.

As a side remark, we want to clarify the terminology used in existing literature. We introduced the specific humidity, which is defined as the ratio of WV mass over total air mass, while the mixing ratio $\chi = \frac{\rho_{wv}}{\rho_{da}}$ is defined as the ratio of WV mass over the mass of the DA. As mentioned before, for atmospheric applications this difference is mostly irrelevant. Nevertheless, it makes sense to apply some rigour and use the correct terminology in contrail formation studies. Using mixing ratio instead of specific humidity, the WV mass conservation equation (the equivalent equation for $q$ is given in Equation (18)) and the prognostic equation (cf. Equation (20)) can be written as

$$\chi_E \, m_{E,DA} + \chi_a \, m_{a,DA}(t) = \chi_{mix}(t) m_{mix,DA}(t) \tag{28}$$

and

$$\frac{d\chi_{mix}}{dt} = \frac{\dot{m}_{DA}}{m_{DA}} \left(\chi_a - \chi_{mix}\right), \tag{29}$$

respectively. In the latter equation, the logarithmic derivative of the mass is called entrainment rate, which typically refers to the total plume mass (as it appears in the equation for $q$, Equation (20)) and not to the DA mass only (as in Equation (29)). While Ref. [8] does neither use the term 'specific humidity' nor 'mixing ratio' and does not distinguish between the two, many other studies have used the term 'mixing ratio' [27, 43–46], where 'specific humidity' would have been more appropriate. Note that Ref. [11] uses specific humidity and refers to it as 'mass fraction'.

## 3.0 Application of the generalised contrail formation theory to future aircraft propulsion systems

This chapter applies the generalised mixing curve as defined by Equation (24) for various potential propulsion systems and fuels of future aircraft. We compare it with the classical mixing line (see Equation (10)) to assess the impact and validity of the assumptions outlined in Section 2.3.

We analyse a wide range of possible future aircraft fuels and propulsion system configurations. The exhaust conditions are varied according to the specific propulsion system being considered. Specifically, four distinct fuel types are examined: kerosene, methane, ammonia and hydrogen. Additionally, the impact of WV and heat recuperation in hydrogen FC systems is investigated. Lastly, ambient conditions are varied for a specific hydrogen FC case to assess the influence of atmospheric conditions. In total, we consider eight cases that are summarised in Table 2. The heat of combustion and WV emission index for the different fuels are given in Table 1. We assume that the initial dilution factor $N_E$ is around 70 in the kerosene case [46]. For all other fuels, $N_E$ is implicitly adjusted such that $Q_{avail}$ is the same for all fuel types. When changing e.g. from kerosene to $H_2$, the fuel consumption would be smaller due to the larger combustion heat. For comparable engine size, exhaust mass flow and $T_E$, this implies an adjustment of

https://doi.org/10.1017/aer.2026.10185 Published online by Cambridge University Press

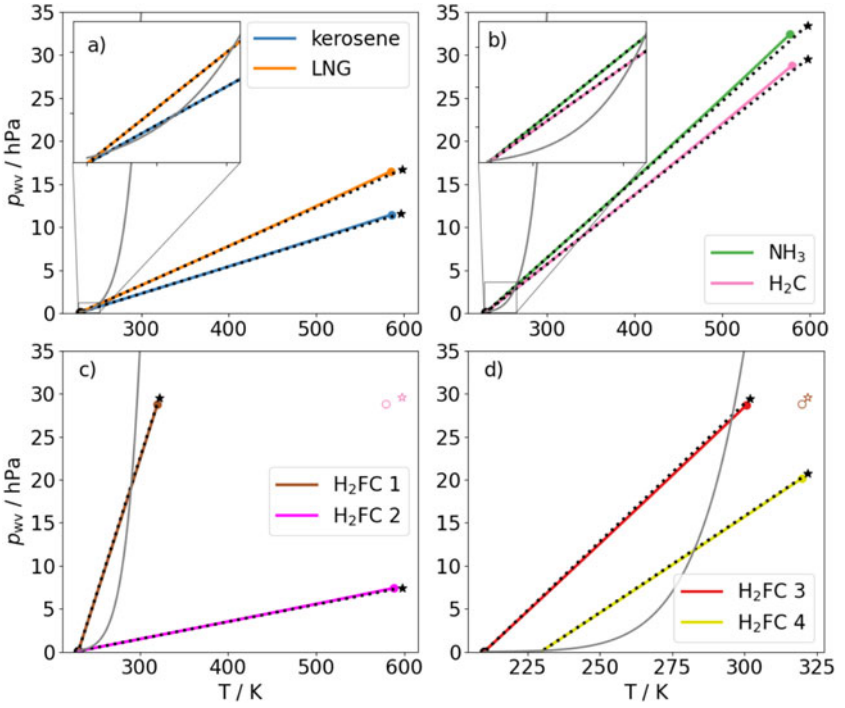


***Figure 4.*** *Comparison between the mixing curve, given by Equation (24), and its respective mixing line (black dotted) for different propulsion systems and fuels (see legend for colours). All cases are outlined in Table 2. The right end points of the mixing curves are indicated by a filled circle, while that of the mixing lines by a black star. The additional pink symbols in panel c show the $H_2C$ case of panel b, the brown ones in panel d show the $H_2FC$ 1 case of panel c.*

$N_E$. The resulting values for $N_E$ in Table 2 might differ from actual air-to-fuel exhaust ratios, because these also depend on the operation state of the engine and the aircraft design. Yet, the plume properties are not much affected by our choice of $N_E$. A smaller $N_E$ leads to larger $T_E$ and $q_E$ values and would simply extend the plotted range, while higher values for $N_E$ lead to lower exhaust values. Both variants do not influence the shape of the mixing curves, leading to the same plume states during mixing as displayed in Fig. 4.

We examine various propulsion systems that may be employed in the coming decades. As the efficiency of these systems is hard to project, a constant value of $\eta = 0.4$ is assumed for all cases. In reality, the propulsion efficiency may vary with fuel type due to differences in combustion behaviour and thermodynamic properties. However, a variation of $\eta$ over a reasonable range has a much smaller impact on plume thermodynamics than a variation of fuel type or the newly introduced factors $\gamma$ and $\delta$. For simplicity, a constant overall propulsion efficiency is assumed. Although the technical realisation of a combustion turbine and a fuel cell are fundamentally different, for our study, only the emitted heat and WV are of interest. Hence, contrail formation is independent of whether the fuel is combusted in a turbine or converted to electric power in an FC. However, we do consider one potential technical advancement that may be feasible for FC systems: the recuperation of heat and WV before the gas is emitted. This could significantly reduce the emitted heat or WV and would clearly influence contrail formation. To account for this, we analyse an FC system, which emits only 25 % of the available energy $Q_{avail}$ as heat while the remaining 75 % are reused within the aircraft ($H_2FC$ 1). Additionally, an FC system is analysed, which only emits 25 % of the produced WV ($H_2FC$ 2), and the remaining 75 % are condensed and

https://doi.org/10.1017/aer.2026.10185 Published online by Cambridge University Press

emitted as liquid droplets, separately from the heated exhaust. Note that this value is purely hypothetical, as no current aircraft systems employ WV condensation to mitigate exhaust humidity. The chosen values represent a range of potential future mitigation scenarios.

Ambient conditions at a relatively low flight level are considered, corresponding to an ambient pressure of $p_a = 400$ hPa and an ambient temperature of $T_a = 230$ K, which corresponds to a temperature that is 10 K lower than the temperature defined by the ISA at this flight level. We choose a low flight level because the technical realisation of fuel-cell-propelled aircraft is currently expected to be implemented for small, regional aircraft, which operate at lower altitudes. Additionally, propeller-driven aircraft require higher air densities than combustion aircraft to operate efficiently and thus fly at lower altitudes. To investigate the impact of atmospheric conditions on the mixing process, two cases with independently reduced ambient temperature $T_a = 210$ K ($H_2$FC 3) and increased flight altitude $p_a = 280$ hPa ($H_2$FC 4) are added. For all cases, the ambient air is assumed to be saturated with respect to ice, i.e. $RH_{i,a} = 100\,\%$ . The exact value of $RH_{i,a}$ has only a very small influence on contrail formation, e.g. [47]. However, contrails can persist only when $RH_{i,a} > 100\,\%$. The occurrence frequency of ISSRs has primarily been studied in the context of current long-haul aircraft, which operate at higher cruising altitudes compared to regional aircraft. Based on findings from [14] and [48], the frequency of ISSRs may be slightly reduced at lower flight altitudes. Nevertheless, such reductions are not sufficient to eliminate the potential for persistent contrails, particularly for low temperatures during winter months.

Figure 4 depicts the mixing curve and its respective mixing line in a Schmidt-Appleman plot for each case listed in Table 2. While each mixing curve is represented by a different colour in Fig. 4, the corresponding mixing lines are all given as dotted black lines. The ambient conditions are represented by a black circle in the lower left corner of all panels, while the initial exhaust conditions are represented by a coloured circle for the general mixing curve and a black star for the classical mixing line. The grey lines represent the saturation pressure over water $p_{w,sat}(T)$. The zoomed-in windows highlight the temperature range relevant for contrail formation, i.e. the temperature range, where the mixing line and curve lie above the saturation pressure curve. The most notable observation across all panels is that the mixing curves closely align with their corresponding mixing lines. Figure 4 reveals that the mixing curves are only slightly curved and can be approximated by their corresponding mixing line.

Figure 4(a) and (b) depict the mixing curves and lines for different fuel types (first four cases in Table 2). Because all cases are constructed to emit the same amount of energy, the exhaust temperatures differ only slightly from one another in the top row. These small differences originate from the differences in heat capacities that depend on the specific humidity of the exhaust. The initial specific humidity $q_E$ varies with fuel type and is lowest for kerosene (blue line, case 'kero'). This example represents a limiting case where the plume is only slightly supersaturated over a very narrow temperature range. For the LNG exhaust (orange line, case 'LNG'), $q_E$ is larger than for kerosene due to the higher WV emission index, resulting in a plume that is clearly supersaturated during mixing. The difference in $q_E$ compared to kerosene is even more pronounced when ammonia or hydrogen is used, leading to a larger slope of the mixing curves and consequently to higher supersaturation values during plume mixing in Fig. 4(b). The mixing curves for ammonia (green line, case 'ammo') and hydrogen (pink line, case '$H_2$C') are very similar, which can be attributed to their similar energy-specific WV emission indices of $\zeta$ (see Table 1). Despite the higher moisture content present in the plumes when using ammonia or hydrogen, the mixing curves do not differ significantly from their respective mixing lines for temperatures where the plume is supersaturated. Figure 4(c) illustrates the effects of heat ('$H_2$FC 1', brown line) and WV ('$H_2$FC 2', magenta line) recuperation of a hydrogen FC-based propulsion system on the mixing process. As a reference, the initial exhaust conditions are shown for the unaltered '$H_2$C' exhaust (cf. Fig. 4(b)). Heat recuperation results in a significant reduction of $T_E$ while leaving $q_E$ unchanged. This leads to a substantial increase in the mixing curve's slope and even larger supersaturation values than in the $H_2$C case. In contrast, WV recuperation leads to a decrease in the mixing curve's slope. For the specific case displayed, this results in a mixing curve that is only slightly supersaturated and lower than in the kerosene case shown in Fig. 4(a). This is expected as $\gamma$ is smaller than $\zeta^{-1}_{norm,H2}$. Figure 4(d) shows the dependence of the mixing curve on the ambient conditions. Note that for this panel, the limit of the temperature

https://doi.org/10.1017/aer.2026.10185 Published online by Cambridge University Press

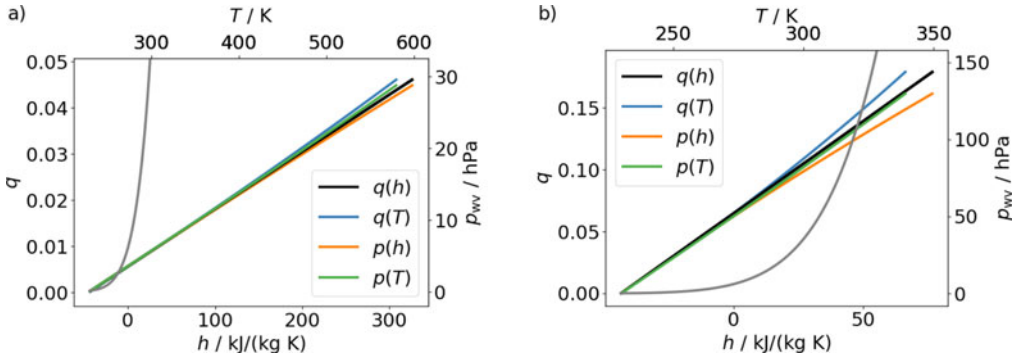


***Figure 5.*** *Comparison of mixing curve and line along different axes for two different cases for hydrogen-powered fuel cell: a) 'H₂FC 1' case, see Tab. 2; b) extreme case:* $\eta_{extr} = 0.5$, $\gamma_{extr} = 1$, $\delta_{extr} = 0.1$, $p_{a,extr} = 400\,hPa$, $T_{a,extr} = 210\,K$.

axis is much smaller than for the other panels, as both cases have a lower initial exhaust temperature. The brown symbols in this panel correspond to the initial exhaust conditions of the case with reduced exhaust heat at unaltered ambient conditions '$H_2$FC 1' as a reference. The red curve ('$H_2$FC 3') illustrates that a decrease in ambient temperature leads to larger supersaturation values. Notably, for the displayed case, the exhaust itself is already nearly saturated. The yellow curve shows the mixing curve at a higher flight level ('$H_2$FC 4'). Due to the lower overall pressure, the WV partial pressure is reduced, resulting in lower supersaturation of the plume during mixing. Under real atmospheric conditions, ambient pressure and temperature do not vary independently, but a decrease in ambient pressure due to a higher flight level is, on average, associated with a decrease in ambient temperature. A simultaneous decrease of ambient pressure and temperature leads to counteracting effects on the mixing curve. Hence, varying only one of the two parameters may slightly overemphasise the sensitivity of the mixing curve slope on ambient conditions.

In general, the lower $q_E$ and the higher $T_E$, the lower the slope of the mixing curve and its supersaturation values. Moreover, Fig. 4 discloses fairly small differences between the classical mixing line and the generalised mixing curve for all considered cases.

Figure 5 provides a detailed explanation of why the two formulations give basically identical results. It shows the mixing curves and lines for two scenarios, which are depicted for four different combinations of coordinate axes, namely $h$ or $T$ on the x-axis and $q$ or $p_{wv}$ on the y-axis. The ranges of the different axes are chosen such that the end and start points of the classical mixing line coincide on both ends for all axes combinations. Using the linear functions $\hat{q}(p_{wv})$ (Equation (9)) and $h(T)$ (Equation (7)) in the classical formulation, the connecting straight line is the same for all four axes combinations, represented by the black line. For non-linear relations (see Equations (13), (15) and (16)), the initial exhaust values differ from those obtained by using their respective linearisation (Equations (9) and (7)). For better assessment of the plume's saturation state, the grey line shows $p_{w,sat}(T)$.

Figure 5(b) illustrates the case '$H_2$FC 1', whose mixing line and curve have already been shown in Fig. 4(b). Both formulations (classical and generalised) are based on the linear $q - h$ relationship and share the same straight (black) line in these coordinate axes. In the $q - T$ diagram, the mixing curve is represented by the blue line, which is slightly convex near the upper initial point and $T_E$ is lower than for the mixing line. This is the effect of the heat capacity being a function of temperature and humidity, resulting in larger values compared to the DA value at constant temperature. Consequently, $T_E$ of the mixing curve is lower for the same $h_E$. In the $p_{wv} - h$ diagram, the mixing curve is represented by the orange line. This curve is slightly concave near the upper point, where the partial pressure is lower compared to the mixing line. This effect originates from the employment of the non-linear Equation (13), which leads to a lower partial pressure for the same specific humidity value. In the $p_{wv} - T$ diagram (green line), both effects are present for the initial exhaust: the lower temperature due to the increased

https://doi.org/10.1017/aer.2026.10185 Published online by Cambridge University Press

heat capacity and the lower WV partial pressure due to the usage of the correct specific humidity definition. The right end points of the mixing line and curve are not the same, but both effects basically cancel each other as the end point of the mixing curve lies almost on the mixing line. For contrail formation, however, not the exact exhaust conditions are relevant; the relationship between $p_{wv}$ and $T$ becomes crucial in the temperature range where the plume reaches supersaturation.

To confirm that the mixing line and mixing curve approaches give, in general, identical results regarding contrail formation, both formulations are compared for an extreme case. This extreme case should meet the following conditions: the initial exhaust should be very moist and its temperature as low as possible. With these conditions, the initial exhaust would have a large relative humidity and a high WV content, resulting in the largest expected differences between the line and the curve within the range where the plume is supersaturated. To meet these conditions, a hydrogen fuel cell case with a 90 % heat recuperation ($\delta_{extr} = 0.1$) is employed, while all of the generated WV is emitted. The efficiency is increased to $\eta_{extr} = 0.5$. The ambient temperature is set to $T_{a,extr} = 210\,\mathrm{K}$ while the pressure is chosen to be $p_{a,extr} = 400\,\mathrm{hPa}$ in an ice-saturated atmosphere. The right end point corresponds to an initial dilution of $N_E = 50$. We want to stress that this is an academic case, meaning that this is used to highlight possible differences between the formulations, and we do not expect that this case will be relevant in practice. Even for this extreme case where the initial exhaust is almost saturated with water, the mixing curve is very similar to the classical mixing line, cf. Fig. 5(b). The temperature range of the extreme case is smaller than for the '$H_2$FC 1' case, while the specific humidity range is larger. The trends are the same as described for Fig. 5(a), but due to the smaller temperature range, the differences are more pronounced. Nevertheless, the resulting green mixing curve aligns with the black mixing line, leading to no difference in the decision whether a contrail forms or not.

The cancellation of two linearisation errors occurs in all cases and leads to almost identical results for the classical mixing line and the mixing curve. This is a surprising, yet comforting, outcome, as it shows that the classical mixing line can be used to assess contrail formation for very moist plumes, despite being based on some potentially inaccurate assumptions.

As a direct consequence, we find that the limiting temperatures $\hat{T}_{lim}$ derived with both formulations are also close to each other. Specifically, $\hat{T}_{lim}$ differs by less than 0.2 K between both formulations for all cases presented in Table 2. This similarity can be attributed to the close alignment of the mixing lines and the generalised mixing curves in the $p_{wv} - T$ diagram as exemplified in Fig. 5, especially in the temperature range where the plume is supersaturated. For the extreme case in Fig. 5(b), $\hat{T}_{lim}$ differs by approximately 0.2 K between both formulations, highlighting that the similarity between both formulations holds for all cases.

We want to stress that the implementation of only one correction of the linear assumptions, without implementing the other correction, can lead to larger inaccuracies than using the classical mixing line. This is shown in Fig. 5(b), where the blue and orange lines differ from the aligned green and black curves. This difference is also reflected in the respective limiting temperatures. Due to the larger curvature of both the orange and the blue line, $\hat{T}_{lim}$ differs by several degrees from the limiting temperature evaluated with the generalised mixing curve. It is essential to note that $\hat{T}_{lim}$ calculated for this extreme case is very high, and discrepancies have likely no practical effect on contrail formation. $\hat{T}_{lim}$ is the critical factor for contrail formation only if $\hat{T}_{lim} < T_{frz}$. If $\hat{T}_{lim}$ exceeds the freezing threshold, contrail formation is instead restricted by $T_{frz}$. The latter occurs in all cases given in Table 2 except for kerosene combustion and the case '$H_2$FC 2'. This suggests that contrail formation will occur as long as the ambient temperature is below the freezing temperature for future aircraft if fuels with high hydrogen content are used without reduction of the WV emissions. This holds only when future aircraft will not have a much lower overall propulsion efficiency than current aircraft (which is not expected).

Having also in mind the computational overhead of determining the mixing curve compared to the mixing line, we conclude that the mixing line is a suitable approximation for the mixing curve even for very moist plumes. The generalised mixing curve is almost identical to the mixing line for all considered cases, and the effect of the generalisation on the limiting temperature can also be neglected. Therefore, the mixing line can be used to investigate contrail formation for future aircraft propulsion systems.

https://doi.org/10.1017/aer.2026.10185 Published online by Cambridge University Press

***Table 3.*** *Overview of relative emission factors $\lambda_i$ to achieve different levels of contrail formation suppression by emission manipulation*

| Variable | Goal | Condition | $\lambda_{H_2}$ |
|---|---|---|---|
| $\lambda_{H_2,\text{ref kero}}$ | Plume thermodynamics comparable to kerosene combustion | $G_{H_2} = G_{\text{kero}}$ | 0.39 |
| $\lambda_{100\,\%}$ | Suppress contrail formation | $RH_w < 100\,\%$ | pink symbols in Figure 6a |
| $\lambda_{500\,\%}$ | Suppress HDN process | $RH_w < 500\,\%$ | pink symbols in Figure 6b |

## 4.0 Technical modifications of the FC exhaust and its effect on contrail formation

In this section, the possibility of contrail avoidance by potential heat and WV recuperation systems in FC-propelled aircraft is investigated. The goal of heat recuperation systems is to increase the efficiency of the propulsion system by using parts of the remaining energy of the gas before emission. In addition, heat exchangers that divert some of the generated heat away from the FC stack are necessary to ensure a constant operating temperature within the stack [21]. While this internal heat management has no direct influence on the exhaust temperature, the usage of heat recovery results in lower exhaust temperatures, leading to plume conditions more favourable for contrail formation. In contrast, WV recuperation leads to less favourable conditions for contrail formation. The extracted WV could be liquefied into water droplets, which are then separated from the heated exhaust. We assume that the released latent heat by liquefying the WV only heats the stream of liquid water and does not increase the temperature of the exhaust. The exhaust heat and the water droplets should be emitted at different locations of the aircraft. Ideally, the droplets would be emitted at a location such that they will not be entrained into the expanding exhaust plume. Note that the following paragraphs do not discuss implicit changes of $\eta$ by technical modifications, but solely focus on changes of the emission factors $\gamma$ and $\delta$.

For contrail avoidance by technical means, the exhaust should contain less water and/or have a higher temperature to decrease the mixing line's slope and thus reduce the contrail formation propensity. Even if contrail formation is not suppressed completely, a drier or hotter plume results in smaller peak relative humidity values and a shorter supersaturation period during mixing. Both effects can reduce the number of ice crystals forming in the first seconds behind the aircraft [27, 46] and the radiative impact of the mature contrail [32–34], which may evolve in suitable environmental conditions.

In the following, we assume that it is technically possible to install heat and WV recuperation systems in an FC-propelled aircraft to manipulate the humidity and temperature of the exhaust. The classical mixing line is used for the following analysis to reduce the computational effort relative to the mixing curve computations. To ensure that the use of hydrogen-based FC systems does not increase the contrail formation propensity, a first goal for contrail mitigation would be to reduce the water emission such that the mixing line of the FC-propelled aircraft's plume aligns with that of an aircraft using kerosene combustion, i.e. we require $G_{H_2} = G_{\text{kero}}$ (first line in Table 3). Assuming equivalent efficiencies for both kerosene and hydrogen propulsion systems, the WV emission has to be reduced by the inverse value of $\zeta_{\text{norm}}$ given in Table 1, i.e. $\gamma_{H_2,\text{ref kero}} = (\zeta_{\text{norm}})^{-1} = 0.39$. However, this value is based on the assumption that no heat is recuperated nor any energy losses occur around the propulsion units, which would reduce $Q_{\text{avail}}$ of the exhaust. To account for heat recuperation, a new variable $\lambda = \gamma/\delta$ is introduced, which represents the relative emission factor of the exhaust. This allows us to calculate the required WV reduction for a given value of heat recuperation. As an exemplary calculation, if 50 % of $Q_{\text{avail}}$ for a $H_2$ propelled aircraft is recuperated, it would require a 78 % reduction of the WV emission to avoid additional contrail formation compared to the kerosene propelled aircraft, because $\lambda_{H_2,\text{ref kero}} = 0.39$.

While the requirement $G_{H_2} = G_{\text{kero}}$ keeps the contrail formation probability of $H_2$FC aircraft at the level of kerosene aircraft (previous paragraph), emission manipulation can be used to further reduce the $H_2$FC contrail formation probability and the associated climate impact of contrail-cirrus. It would be beneficial to completely suppress contrail formation by technical modification of the exhaust, by requiring that the plume $RH_w$ remains below 100 % (second line in Table 3). Such a controlled exhaust

https://doi.org/10.1017/aer.2026.10185 Published online by Cambridge University Press

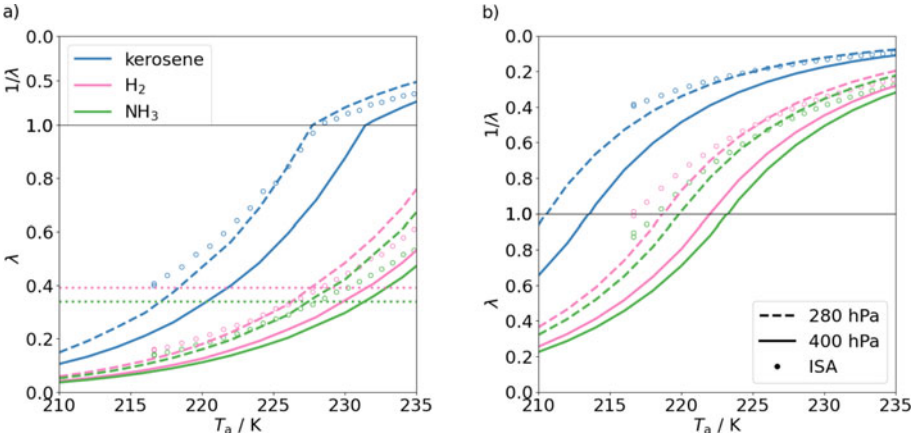


***Figure 6.*** *Ratio between heat and WV recuperation λ to limit the maximum relative humidity during plume mixing for different fuels and ambient. The lower part of the plots shows λ, while the upper part shows* $1/\lambda$ *if* $\lambda > 1$. *a) No contrail forms:* $\lambda_{100\,\%}$ *b) No HDN occurs:* $\lambda_{500\,\%}$.

modification, which may be associated with extra costs, is only required when flying in ISSRs. This proposition is similar to the idea of a targeted use of SAFs [49]. In both concepts, contrail formation is on-demand technically modified. The maximum λ value is calculated, for which supersaturation with respect to water during mixing is avoided. This critical value $\lambda_{100\,\%}$ depends on atmospheric conditions and is smaller (i.e. technically more demanding) than $\lambda_{\text{ref kero}}$ for cases where a kerosene contrail would form and less demanding when no kerosene contrail would form. In the limiting case for contrail formation, the relative humidity of the plume is at most $\text{RH}_{\text{w,max}} = 100\,\%$ during the whole mixing process. We perform an iterative search of the mixing line slope necessary for the mixing line to be tangential to $p_{\text{w,sat}}(T)$. The resulting mixing line slope can then be used to calculate the corresponding relative emission factor $\lambda = \gamma/\delta$ via Equation (4).

Figure 6(a) shows $\lambda_{100\,\%}$ as a function of ambient temperature for different fuels and two different flight levels at $p_{\text{a}} \in \{280, 400\}$ hPa. In addition to the two constant pressure levels, the circles in Fig. 6 use $p_{\text{a}}(T_{\text{a}})$ as given by the ISA. The dotted horizontal lines indicate the relative emission fraction $\lambda_{\text{i,ref kero}}$ necessary to restrict contrail formation to those scenarios where kerosene combustion would produce a contrail. For $\lambda_{100\,\%} > 1$, the unaltered exhaust would not form a contrail for the specified ambient conditions. Therefore, heat reduction can be applied up to $\delta = 1/\lambda_{100\,\%}$ with the unaltered water emission without forming a contrail for these cases. Figure 6(a) reveals that this occurs only when kerosene is used as a fuel because $\hat{T}_{\text{lim}} > 235$ K for hydrogen and ammonia. For all fuels, $\lambda_{100\,\%}$ increases with increasing ambient temperatures and decreasing ambient pressure. For identical ambient conditions, the $\lambda_{100\,\%}$ curves for different fuels differ simply by a factor identical to the ratio of $\zeta^{-1}$. This indicates that contrail avoidance requires more WV extraction for the same amount of recovered heat when ammonia is used instead of pure hydrogen. In general, the higher $\lambda_{100\,\%}$ values for higher ambient temperatures make contrail avoidance easier for FC-propelled regional aircraft, as their lower flight altitude leads on average to higher ambient temperatures.

Nonetheless, especially for low $T_{\text{a}}$, the $\lambda_{100\,\%}$ values are small, making it challenging to implement recuperation systems that can effectively meet this goal. If a complete suppression of contrail formation for FC-propelled aircraft is out of reach in a technical sense, it may still be beneficial to keep the peak humidity below a certain (technically less demanding) limit. As discussed above, heat recuperation leads to a decrease in exhaust temperature and consequently to an increase in the maximum relative humidity. Hence, heat recuperation without the use of WV reduction can lead to relative humidity values above 500 % during plume mixing, if fuels with high hydrogen content like hydrogen or ammonia are used (third line in Table 3).

https://doi.org/10.1017/aer.2026.10185 Published online by Cambridge University Press

For these very high supersaturation values, an additional droplet-forming process can become significant: homogeneous droplet nucleation (HDN). This process condenses WV directly from the vapour phase into nanometer-sized droplets without the need for condensation particles. HDN commonly occurs in steam turbines [50] and can also lead to the formation of aerodynamic contrails [51] over aircraft wings in cold conditions. Based on theoretical and experimental results, Ref. [52] provides an empirical correlation of the nucleation rate with temperature and supersaturation. This correlation fits most experimental findings well, as shown in Fig. 3 of Ref. [51]. For typical plume temperatures at which supersaturation occurs, the nucleation rate of HDN is negligible for relative humidity values below 500 % , but increases in a highly non-linear fashion with both supersaturation and temperature. For $RH_{w,max} \gtrsim 500\ \%$ , it cannot be ruled out that the droplet and consequently ice crystal numbers increase substantially compared to hydrogen plumes with $RH_{w,max} < 500\ \%$. It cannot be excluded that ice crystal numbers might even be higher than in typical soot-rich kerosene combustion scenarios as studied in Ref. [53]. This effect would come along with increased contrail formation propensity in lower flight levels due to the higher limiting temperature of hydrogen compared to kerosene. The combination of both effects (higher contrail formation propensity and more ice crystals) would increase the climate impact of contrail-cirrus formed behind hydrogen FC-based aircraft.

Analogously to $\lambda_{100\,\%}$ , $\lambda_{500\,\%}$ is defined as the maximum $\lambda$ value for which the peak relative humidity within the plume is kept below 500 % during mixing. Similar in style to panel 6(a), Figure 6(b) depicts $\lambda_{500\,\%}$ . As expected, $\lambda_{500\,\%}$ values are larger than the respective $\lambda_{100\,\%}$ values, i.e. less WV has to extracted from the exhaust to remain below 500 % . The trends in both panels are similar, with the curves in panel 6(b) shifted towards higher values of $\lambda$. Nevertheless, for low ambient temperatures, it is still necessary to reduce WV emissions to suppress HDN, especially when hydrogen or ammonia is used. For kerosene with unaltered exhaust (i.e. $\lambda = 1$), we observe $RH_{w,max} > 500\ \%$ only for very low ambient temperature values. Additionally, for the kerosene case, the high number of emitted soot particles leads to a fast depletion of WV and the actual $RH_w$ values in the plume are much smaller than the theoretical peak value without considering microphysics (as done in the present study). For hydrogen plumes being void of soot particles and under the assumption of ice crystal formation on entrained ambient aerosol [27], WV is depleted more slowly and the $RH_w$ values with and without considering microphysics can be more similar. Reference [27] presented contrail formation simulations for hydrogen combustion, and the plume thermodynamic properties correspond to our hydrogen case with $\gamma = \delta = 1$. Even though condensation/deposition depletes the WV, the peak relative humidity increases with decreasing $T_a$ and can reach values up to 500 % . Hence, for hydrogen scenarios, $RH_{w,max}$ could be a good indicator whether or not HDN may occur. The present study will not provide quantitative estimates on how many additional ice crystals may form by HDN. This work is deferred to an upcoming simulation study introducing the HDN process in the contrail formation model described in Ref. [27].

Figure 7 shows the maximum relative humidity $RH_{w,max}$ during plume mixing for various fuels, considering $\lambda$ values between 0.2 and 2 and ambient temperatures below the freezing temperature. The ambient relative humidity is set to $RH_{i,a} = 100\ \%$ and the ambient pressure is set to $p_a = 400$ hPa, which relates to a relatively low flight level. It has to be noted that for this flight level, ambient temperatures $T_a \leq 220$ K occur only rarely. The white area in each panel indicates the region where no contrail forms, i.e. $RH_{w,max} < 100\ \%$. The white curve in each panel represents the condition where $RH_{w,max} = 500\ \%$ . It is possible that HDN will be triggered if the plume conditions are located to the right of this curve. For kerosene, the maximum relative humidity remains below 500 % except for very cold ambient conditions, which are unlikely at this pressure level. In contrast, the area where $RH_{w,max} > 500\ \%$ is significantly increased for hydrogen and ammonia. Additionally, the maximum relative humidity can reach $RH_{w,max} = 4000\ \%$ for ammonia if $\lambda \geq 2$. Note that the leftmost panel on kerosene is not overly meaningful, as for soot-rich conditions, the actual $RH_{w,max}$ values are much smaller when condensation/evaporation is considered. Nevertheless, this plot is included to showcase the general pattern and how it changes when switching to fuels with a larger energy-specific WV emission index. In general, this plot highlights the importance of water recuperation for FC systems to prevent the formation of contrails with potentially substantially increased ice crystal numbers due to HDN.

https://doi.org/10.1017/aer.2026.10185 Published online by Cambridge University Press

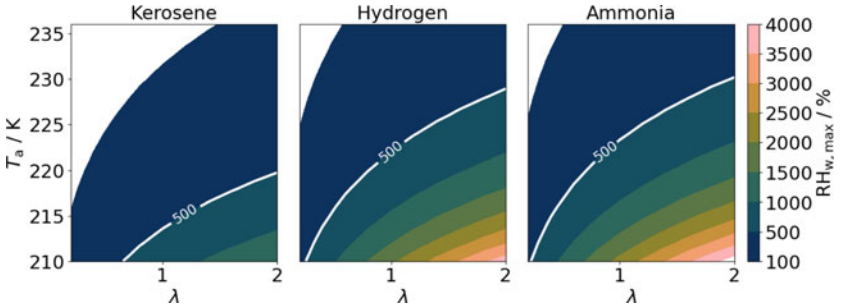


***Figure 7.*** *Maximum relative humidity of the plume at various ambient temperature values and λ values for an FC setup, when using (a) kerosene (b) hydrogen (c) ammonia.* $p_a = 400\,hPa, RH_{i,a} = 100\,\%$.

## 5.0 Discussion

### *5.1 Implications of the generalised mixing curve formulation*

The generalised mixing curve derived in Section 2 aligns well with the classical mixing line for the range of future propulsion systems considered in this study. The usage of different fuels is investigated, and additionally, hydrogen FC-based propulsion with technically altered thermodynamic exhaust properties is considered. Recently, Ref. [11] developed a generalised contrail formation theory to describe the mixing curve for different propulsion systems. Specifically, Richardson's Equation (36) provides the mixing curve slope as a function of the plume mass mixing ratio, leading to a slightly curved plume evolution in the $p_{wv} - T$ diagram. Both our and Richardson's mixing curve formulations disregard any intra-plume gradients and assume a fully mixed plume that can be represented by a single mixed air parcel by the time contrail formation processes become important. However, it is not clear whether this assumption still holds for future turbo-fan systems with high bypass ratios. Equation (36) in Ref. [11] additionally accounts for the kinetic energy of the plume, which results in initially slightly lower exhaust temperatures for the same amount of emitted energy. On the other hand, we use the accurate calculation of the partial pressure from the specific humidity, while Ref. [11] uses the linearised approximation. The dependence of heat capacity on both specific humidity and temperature is included in both our and Richardson's formulation.

The mixing curves presented in Ref. [11] show the same trend as the curves presented in this study. The exhaust values calculated by a generalised formulation, either ours or the one given in Ref. [11], differ from the exhaust values calculated by the classical theory. Within the temperature range relevant for contrail formation, however, the plume conditions evaluated with the generalised formulation do not differ significantly from the classical mixing line. In Richardson's Table 2, the quantities $T_{\mathrm{min}}$ and $T_{\mathrm{max}}$ refer to limiting temperature values for ambient air with $\mathrm{RH}_{\mathrm{w,a}} = 0\,\%$ and $100\,\%$, respectively, and are given for different propulsion systems using kerosene or hydrogen. These temperatures were evaluated using various formulations of the mixing curve, ranging from the classical mixing line to a semi-perfect gas model that accounts for changes in the heat capacity, similar to our analysis. For some cases, especially when using hydrogen, the difference in these limiting temperatures using the various models is not negligible. Notably, these differences in limiting temperature $T_{\mathrm{lim}}$ are most pronounced for $T_{\mathrm{lim}} > T_{\mathrm{frz}}$. For such high limiting temperatures, contrail formation is, however, restricted by $T_{\mathrm{frz}}$, and $T_{\mathrm{lim}}$ has no effect on the binary criterion whether or not contrail formation occurs. For all cases in Ref. [11] where $T_{\mathrm{lim}} < T_{\mathrm{frz}}$, the differences calculated by the various mixing curve formulations are negligibly small. This suggests that the discrepancies in $T_{\mathrm{lim}}$ between different mixing curve formulations have no practical impact on the contrail formation criterion, which is consistent with our findings.

Even though the initial exhaust conditions appear explicitly in the generalised mixing curve (Equation (24)), our results are not presented in terms of exhaust conditions close to the exit. Instead, the overall energy and WV budget is considered, and relative emission factors $\gamma$ and $\delta$ are introduced in Equation (4). This formula requires the overall propulsion efficiency as input, which might be difficult to

https://doi.org/10.1017/aer.2026.10185 Published online by Cambridge University Press

obtain or even be unavailable for future fuel cell configurations. Alternatively, one could provide exhaust conditions at the exit (or any downstream location close to it) to directly plug it into Equation (24). For given values of $q_E$, $h_E$, $EI_{H_2O}$ and $Q$, one can compute

$$\lambda' := \frac{\gamma}{\delta\,(1-\eta)} = \frac{q_E}{h_E}\frac{Q}{EI_{H_2O}} \tag{30}$$

to make the connection to our analysis. In essence, it is not necessary to know each factor individually. Determining $\lambda'$ is sufficient to enable a comparative analysis of contrail formation between fuel cell propulsion systems and conventional combustion-based propulsion systems.

While we provide a formulation for the slope that depends linearly on $\lambda$, the slope in Ref. [9] depends sensitively on the voltage used in the FC. The choice of the voltage implicitly determines the efficiency of the FC, which is not varied explicitly in our study (but a change of $\eta$ can be translated into a change in $\lambda$). The two voltages (0.5 V and 1 V) used in Ref. [9] correspond to $\eta = 0.41$ and $\eta = 0.82$, respectively. The efficiency associated with 0.5 V is close to our assumption $\eta = 0.4$ and the efficiency values for modern kerosene combustion engines. On the other hand, $\eta \approx 0.8$ is a rather theoretical assumption and is not expected to be achievable for FC stacks in aircraft. Therefore, the large mixing line slopes in Ref. [9] associated with a voltage of 1 V will not be reached for FC-propelled aircraft.

### *5.2 Implications of technically manipulated exhaust properties*

We assume that parts of the available energy released by the FC system will be recuperated and used to increase the overall system efficiency. Lower exhaust temperatures due to heat recuperation could lead to the situation that the gas is supersaturated prior to its emission, and condensation of water could occur inside the pipes. Consequently, liquid water droplets could be emitted together with the moist exhaust. These emitted water droplets would reduce the supersaturation in the plume in a similar manner to solid particle emissions. A lower exhaust temperature of the plume leads to higher relative humidity values during plume mixing. These do not necessarily lead to an increased number of formed ice crystals if no additional particles are activated into water droplets. However, if the relative humidity exceeds a certain threshold, HDN could be triggered, which potentially produces many small water droplets exceeding the abundance in typical contrails. Figure 7 shows that the relative humidity values necessary to trigger this process could be surpassed when heat recuperation is implemented.

It is essential to emphasise that the results presented here are purely thermodynamical, and no microphysical processes are considered. Consequently, the maximum relative humidity values shown in Fig. 7 are upper estimates. They would be lower when microphysics is taken into account. Plume WV is depleted by condensation once the plume becomes supersaturated, reducing the relative humidity. This effect is particularly pronounced for current kerosene combustion, where large numbers of soot particles are emitted that can be activated into water droplets and thereby reduce the supersaturation of the plume. In contrast, FC propulsion systems are expected to emit significantly fewer particles (no soot present), thereby reducing the condensation effect. Consequently, our analysis can be seen as a limiting scenario, where no WV-depleting particles are present in the plume. It has to be noted that the likelihood of triggering HDN is highest for very low ambient temperatures. As FC-propelled aircraft are expected to fly at relatively low altitudes, very low ambient temperature values will be encountered less often than for current aircraft. This reduces the likelihood of encountering ambient conditions that lead to the highest $RH_{w,max}$ values given in Fig. 7 and therefore the relevance of HDN may not be as large as suggested by this figure. Nevertheless, is it necessary to investigate the possible onset of HDN quantitatively to assess its impact on contrail properties of very moist plumes. This is not possible with a purely thermodynamic model, but requires numerical models that capture all relevant microphysical processes.

While heat reduction of the exhaust gas leads to a higher contrail formation propensity, manipulation of the exhaust can also be employed to reduce the contrail formation propensity for FC-propelled aircraft. A complete suppression of contrail formation could be achieved by keeping $RH_w \leq 100\,\%$ during dilution because this prevents the formation of water droplets. As indicated in Fig. 1(b), WV condensers

https://doi.org/10.1017/aer.2026.10185 Published online by Cambridge University Press

may be introduced to condense a portion of the produced WV. Ideally, large liquid droplets are released at a location where they are not entrained and do not re-moisturise the expanding exhaust. The climatic effect of such large droplets is expected to be small, as they fall out quickly. Figure 1(b) also implies that the exhaust need not be emitted into the propeller wake, enabling strategic placement to potentially modify plume dilution and contrail formation processes. If a large fraction of the produced heat is permanently diverted from the exhaust, high supersaturations may occur during plume dilution with undesired effects on contrail formation. It would be beneficial to design an aircraft for which as much of the diverted heat as possible mixes with the exhaust, either before or after its release. If WV recuperation systems were able to significantly decrease the WV amount and maintain sub-saturation in the diluting plume, this would have a substantial impact on the reduction of the radiative forcing of contrail-cirrus. Implementing recuperation systems will likely increase the overall complexity of the propulsion system. Our study shows that these recuperation systems could have a significant effect on the contrail formation propensity and consequently on the climate effect of contrail-cirrus.

We explicitly want to state that aircraft design provides leverage for optimising exhaust properties with regard to the contrail climate impact. Our study aims to encourage manufacturers to explore the technical feasibility of installing heat and WV recuperation systems on future FC-propelled aircraft.

## 6.0 Conclusion

This study deals with the thermodynamic theory of contrail formation and investigates under which conditions contrails do or do not form, considering various possible future propulsion systems. The effect on contrail formation propensity of using various fuels like kerosene, LNG, ammonia or pure hydrogen to propel future aircraft is assessed. Additionally, we analyse how the installation of heat and WV recuperation systems installed in hydrogen-based FC systems would change the contrail formation propensity.

The Schmidt-Appleman criterion states whether plume supersaturation and contrail formation occur during plume mixing and is based on a well-established mixing line formulation [8]. To generalise this approach, first the underlying assumptions of the mixing line formulation are scrutinised, which we deem not a-priori justifiable for plumes that, compared to current kerosene exhausts, exhibit lower temperatures and contain more WV.

In a second step, a generalised form of a contrail formation criterion is derived, where several linearisations are dropped, on which the mixing line formulation is based. Specifically, it accounts for the non-linear relation between specific humidity and WV partial pressure. Additionally, a non-constant heat capacity of moist air is included that varies with humidity and temperature, rather than using a fixed heat capacity value of DA. While the classical mixing line features a straight mixing line in the $p_{\mathrm{wv}} - T$ space, the generalised framework results in a mixing curve with a non-constant slope. The generalised formulation is computationally more demanding to solve than the classical mixing line because the functional relationship between temperature and WV partial pressure is more intricate. For given plume temperature $T$, the plume WV partial pressure $p_{\mathrm{wv}}(T)$ can be directly evaluated (see Equation (24)). Moreover, an iterative method is used to determine the limiting temperature, which provides the ambient temperature above which no contrail forms, using the generalised mixing curve.

The generalised mixing curve is compared with the classical mixing line for propulsion systems utilising various fuels and hydrogen-based FC systems. We find that the mixing curve does in no case differ significantly from the classical mixing line. Additionally, the limiting temperature for a specific propulsion system does not change when using the classical mixing line instead of the generalised formulation. Our results are in line with recent results from Ref. [11], who presented a similar formulation of the mixing curve for a wide range of propulsion systems. We also provide an explanation for these small differences between the classical mixing line and the generalised formulation. We find that the errors introduced by the two linear relationships during the derivation of the mixing line lead to an overestimation of both temperature and WV partial pressure at the time of emission. The simultaneous

https://doi.org/10.1017/aer.2026.10185 Published online by Cambridge University Press

increase for both variables leads to a similar shape of the mixing line and the generalised mixing curve and is no longer important by the time the plume becomes supersaturated. Therefore, dropping both linearisation leads to no significant difference because the effects cancel each other. One note of caution: if the classical theory were extended by dropping just one of the two linearisations, the resulting contrail formation criterion would be less accurate than the classical theory. The differences between the mixing line and the generalised formulation are negligible, and the calculation of the mixing line is computationally less expensive. It can be concluded that the classical mixing line formulation produces reliable predictions of contrail formation also for very moist plumes, even though the initial plume properties do not comply with the underlying assumptions.

Hence, the classical mixing line is applied to investigate the influence on contrail formation propensity of possible recuperation systems for future FC-propelled aircraft. Heat recuperation increases the contrail formation propensity by decreasing the exhaust temperature, while WV recuperation decreases contrail formation propensity by decreasing the moisture content within the exhaust. We provide values for technical WV emission reduction necessary to avoid contrail formation when kerosene, ammonia or pure hydrogen is used as a fuel. If it were possible to manipulate the exhaust conditions such that no contrail forms, especially in ISSRs, this would reduce the climate impact of contrail-cirrus for future aircraft significantly. As recuperation systems are not commonly used on current aircraft, we give some indication of the requirements of these systems to mitigate contrail formation.

Additionally, the maximum relative humidity that can be reached within the plume for various relative emission factors is investigated, again when using kerosene, ammonia and pure hydrogen. Reducing the exhaust heat for constant WV emission ($\lambda > 1$) leads to very high relative humidity values during plume mixing when the number of condensation nuclei in the plume is small. This could trigger HDN, a microphysical process that leads to the formation of large numbers of water droplets without the need for nucleation particles. If these droplets freeze in cold ambient conditions, the number of formed ice crystals could increase compared to a comparable aircraft that does not use heat recuperation. The higher number of ice crystals would lead to an increased climate effect of such aircraft due to the increased radiative forcing of persistent contrail-cirrus [34]. Therefore, we present an assessment of the requirements for potential recuperation systems to ensure that HDN is not triggered during plume mixing.

For a quantitative evaluation of the impact of possible HDN events during plume mixing on contrail properties, a numerical model that simulates all relevant microphysical processes during contrail formation is needed. Therefore, our next goal is to extend the Lagrangian Cloud Module box model [46] to include the effects of HDN and simulate the impact on contrail properties.

**Acknowledgements.** This work has been funded by the DLR internal projects H2EAT and H2CONTRAIL. Both authors received funding from Airbus SAS within the framework of understanding contrails from hydrogen propulsion. We thank Klaus Gierens for an internal review of the paper draft and the reviewers for their constructive comments.

## References

[1] Lee, D., Fahey, D., Skowron, A., Allen, M., Burkhardt, U., Chen, Q., Doherty, S., Freeman, S., Forster, P., Fuglestvedt, J., Gettelman, A., De León, R., Lim, L., Lund, M., Millar, R., Owen, B., Penner, J., Pitari, G., Prather, M., Sausen, R. and Wilcox, L. The contribution of global aviation to anthropogenic climate forcing for 2000 to 2018, *Atmos. Environ.*, 2021, **244**, p 117834. https://doi.org/10.1016/j.atmosenv.2020.117834

[2] Eurocontrol. Eurocontrol forecast update 2024-2030. https://www.eurocontrol.int/publication/eurocontrol-forecast-2024-2030-autumn-update. Accessed: 2025-03-12.

[3] European Commission, Directorate-General for Mobility, Transport, Directorate-General for Research, and Innovation. Flightpath 2050 – Europe's vision for aviation – maintaining global leadership and serving society's needs. Publications Office, 2011. https://doi.org/doi/10.2777/50266

[4] Lee, D., Allen, M., Cumpsty, N., Owen, B., Shine, K. and Skowron, A. Uncertainties in mitigating aviation non-CO2 emissions for climate and air quality using hydrocarbon fuels, *Environ. Sci. Atmos.*, 2023, **3**, pp 1693–1740. https://doi.org/10.1039/D3EA00091E

[5] Wilhelm, L., Gierens, K. and Rohs, S. Weather variability induced uncertainty of contrail radiative forcing, *Aerospace*, 2021, **80**, (11). https://doi.org/10.3390/aerospace8110332

[6] Appleman, H. The formation of exhaust condensation trails by jet aircraft, *Bull. Am. Meteorol. Soc.*, 1953, **340**, (1), pp 14–20.

https://doi.org/10.1017/aer.2026.10185 Published online by Cambridge University Press

[7] Schmidt, E Die Entstehung von Eisnebel aus den Auspuffgasen von Flugmotoren, *Schriften der Deutschen Akademie der Luftfahrtforschung*, 1941, **44**, pp 1–15.
[8] Schumann, U. On conditions for contrail formation from aircraft exhausts, *Meteorol. Z.*, 1996, **5**, pp 4–23. https://doi.org/10.1127/metz/5/1996/4
[9] Gierens, K. Theory of contrail formation for fuel cells, *Aerospace*, 2021, **80**, (6). https://doi.org/10.3390/aerospace8060164.
[10] Yin, F., Grewe, V. and Gierens, K. Impact of hybrid-electric aircraft on contrail coverage, *Aerospace*, 2020, **70**, (10). https://doi.org/10.3390/aerospace7100147
[11] Richardson, E. Contrail formation criterion for assessment of alternative propulsion technologies, *J. Propul. Power*, 2025, **410**, (3), pp 264–276. https://doi.org/10.2514/1.B39430
[12] Hofer, S., Gierens, K. and Rohs, S. Contrail formation and persistence conditions for alternative fuels, *Meteorol. Z.*, 2024, **33**, pp 43–49. https://doi.org/10.1127/metz/2024/1178
[13] Dischl, R., Sauer, D., Voigt, C., Harlaß, T., Sakellariou, F., Märkl, R., Schumann, U., Scheibe, M., Kaufmann, S., Roiger, A., Dörnbrack, A., Renard, C., Gauthier, M., Swann, P., Madden, P., Luff, D., Johnson, M., Ahrens, D., Sallinen, R., Schripp, T., Eckel, G., Bauder, U. and Le Clercq, P. Measurements of particle emissions of an A350-941 burning 100 % sustainable aviation fuels in cruise, *Atmos. Chem. Phys.*, 2024, **240**, (19), pp 11255–11273. https://doi.org/10.5194/acp-24-11255-2024
[14] Kaufmann, S., Dischl, R. and Voigt, C. Regional and seasonal impact of hydrogen propulsion systems on potential contrail cirrus cover, *Atmos. Environ.*, 2024, **24**, p 100298. https://doi.org/10.1016/j.aeaoa.2024.100298
[15] Megill, L. and Grewe, V. Investigating the limiting aircraft-design-dependent and environmental factors of persistent contrail formation, *Atmos. Chem. Phys.*, 2025, **250**, (7), pp 4131–4149. https://doi.org/10.5194/acp-25-4131-2025
[16] Soleymani, M., Mostafavi, V., Hebert, M., Kelouwani, S. and Boulon, L. Hydrogen propulsion systems for aircraft, a review on recent advances and ongoing challenges, *Int. J. Hydrog. Energy*, 2024, **91**, pp 137–171. https://doi.org/10.1016/j.ijhydene.2024.10.131
[17] Marciello, V., Stasio, M., Ruocco, M., Trifari, V., Nicolosi, F., Meindl, M., Lemoine, B. and Caliandro, P. Design exploration for sustainable regional hybrid-electric aircraft: a study based on technology forecasts, *Aerospace*, 2023, **100**, (2). https://doi.org/10.3390/aerospace10020165
[18] Gierens, K., Sausen, R., Bauder, U., Eckel, G., Großmann, K., LeClercq, P., Lee, D., Rauch, B., Sauer, D., Voigt, C. and Schmidt, A. Influence of aviation fuel composition on the formation and lifetime of contrails - a literature review, 2024. https://elib.dlr.de/202458/
[19] Tiwari, S., Pekris, M. and Doherty, J. A review of liquid hydrogen aircraft and propulsion technologies, *Int. J. Hydrog. Energy*, 2024, **57**, pp 1174–1196. https://doi.org/10.1016/j.ijhydene.2023.12.263
[20] Ansell, P. Review of sustainable energy carriers for aviation: benefits, challenges, and future viability, *Prog. Aerosp. Sci.*, 2023, **141**, p 100919. https://doi.org/10.1016/j.paerosci.2023.100919
[21] Kazula, S., de Graaf, S. and Enghardt, L. Review of fuel cell technologies and evaluation of their potential and challenges for electrified propulsion systems in commercial aviation, *J. Glob. Power Propuls. Soc.*, 2023, **7**, pp 43–57. https://doi.org/10.33737/jgpps/158036
[22] Frey, A., Bosak, D., Madrid, E., Stonham, J., Sangan, C. and Pountney, O. Thermal management in high temperature proton exchange membrane fuel cells for aircraft propulsion systems, *Prog. Aerosp. Sci.* https://doi.org/10.1016/j.paerosci.2024.101052
[23] Massaro, C., Pramotton, S., Marocco, P., Monteverde, A. and Santarelli, M. Optimal design of a hydrogen-powered fuel cell system for aircraft applications, *Energy Convers. Manage.*, 2024, **306**, p 118266. https://doi.org/10.1016/j.enconman.2024.118266
[24] Adler, J. and Martins, R. Hydrogen-powered aircraft: fundamental concepts, key technologies, and environmental impacts, *Prog. Aerosp. Sci.*, 2023, **141**, p 100922. https://doi.org/10.1016/j.paerosci.2023.100922. Special Issue on Green Aviation.
[25] Märkl, R., Voigt, C., Sauer, D., Dischl, R., Kaufmann, S., Harlaß, T., Hahn, V., Roiger, A., Weiß-Rehm, C., Burkhardt, U., Schumann, U., Marsing, A., Scheibe, M., Dörnbrack, A., Renard, C., Gauthier, M., Swann, P., Madden, P., Luff, D., Sallinen, R., Schripp, T. and Le Clercq, P. Powering aircraft with 100 % sustainable aviation fuel reduces ice crystals in contrails, *Atmos. Chem. Phys.*, 2024, **240**, (6), pp 3813–3837. https://doi.org/10.5194/acp-24-3813-2024
[26] DLR press release for Blue Condor Campaign. https://www.dlr.de/en/latest/news/2025/world-first-in-flight-measurements-of-contrails-from-hydrogen-propulsion. Accessed: 2025-06-25.
[27] Bier, A., Unterstrasser, S., Zink, J., Hillenbrand, D., Jurkat-Witschas, T. and Lottermoser, A. Contrail formation on ambient aerosol particles for aircraft with hydrogen combustion: a box model trajectory study, *Atmos. Chem. Phys.*, 2024, **240**, (4), pp 2319–2344. https://doi.org/10.5194/acp-24-2319-2024
[28] Zink, J., Unterstrasser, S. and Burkhardt, U. Contrail formation for aircraft with hydrogen combustion – part 1: a systematic microphysical investigation, *Atmos. Chem. Phys.*, 2026, **260**, (4), pp 3125–3143. https://doi.org/10.5194/acp-26-3125-2026
[29] Zink, J. and Unterstrasser, S. Contrail formation for aircraft with hydrogen combustion – part 2: Engine-related aspects, *Atmos. Chem. Phys.*, 2026, **260**, (4), pp 3145–3165. https://doi.org/10.5194/acp-26-3145-2026
[30] Zink, J., Unterstrasser, S. and Jurkat-Witschas, T. On the potential role of lubrication oil particles in contrail formation for kerosene and hydrogen combustion, *J. Geophys. Res.*, 2025a, **1300** (12). https://doi.org/10.1029/2025jd043487
[31] Ponsonby, J., King, L., Murray, B. and Stettler, M. Jet aircraft lubrication oil droplets as contrail ice-forming particles, *Atmos. Chem. Phys.*, 2024, **240**, (3), pp 2045–2058. https://doi.org/10.5194/acp-24-2045-2024
[32] Unterstrasser, S. and Gierens, K. Numerical simulations of contrail-to-cirrus transition - part 2: impact of initial ice crystal number, radiation, stratification, secondary nucleation and layer depth, *Atmos. Chem. Phys.*, 2010, **100**, (4), pp 2037–2051. https://doi.org/10.5194/acp-10-2037-2010

https://doi.org/10.1017/aer.2026.10185 Published online by Cambridge University Press

[33] Burkhardt, U., Bock, L. and Bier, A. Mitigating the contrail cirrus climate impact by reducing aircraft soot number emissions, *NPJ Clim. Atmos. Sci.*, 2018, **10**, (1), p 37. https://doi.org/10.1038/s41612-018-0046-4
[34] Lottermoser, A. and Unterstrasser, S. Modeling the impact of alternative fuels and hydrogen propulsion on contrail-cirrus: a parameter study, *J. Geophys. Res.*, 2026, **1310**, (2), p e2025JD044604. https://doi.org/10.1029/2025JD044604
[35] Lewellen, D. Persistent contrails and contrail cirrus. Part 2: full lifetime behavior, *J. Atmos. Sci.*, pp 4420–4438, 2014. https://doi.org/10.1175/JAS-D-13-0317.1
[36] Unterstrasser, S., Gierens, K., Sölch, I. and Lainer, M. Numerical simulations of homogeneously nucleated natural cirrus and contrail-cirrus. Part 1: How different are they? *Meteorol. Z.*, 2017, **260**, (6), pp 621–642. https://doi.org/10.1127/metz/2016/0777
[37] Gierens, K., Schumann, U., Helten, M., Smit, H. and Wang, P. Ice-supersaturated regions and subvisible cirrus in the northern midlatitude upper troposphere, *J. Geophys. Res.*, 2000, **105**, p 22.
[38] Spichtinger, P., Gierens, K. and Wernli, H. A case study on the formation and evolution of ice supersaturation in the vicinity of a warm conveyor belt's outflow region, *Atmos. Chem. Phys.*, 2005, **50**, (4), pp 973–987.
[39] Krempus, D., Beltrame, F., Majer, M., de Servi, C. and Vos, R. ORCWaste heat recovery system for the turboshaft engines of turboelectric aircraft. 2023. https://doi.org/10.13009/EUCASS2023-658. Aerospace Europe Conference 2023: Joint 10th EUCASS - 9th CEAS Conference, 10th EUCASS - 9th CEAS Conference; Conference date: 09-07-2023 through 13-07-2023.
[40] Xu, Y., Tang, H., Chen, M. and Duan, F. Optimization and design of heat recovery system for aviation, *Appl. Therm. Eng.*, 2020, **165**, p 114581. https://doi.org/10.1016/j.applthermaleng.2019.114581
[41] Bücker, D., Span, R. and Wagner, W. Thermodynamic property models for moist air and combustion gases, *J. Eng. Gas Turbine Power*, 2002, **1250**, (1), 374–384. https://doi.org/10.1115/1.1520154
[42] Zink, J. and Unterstrasser, S. Contrail formation for aircraft with hydrogen combustion - part 2: engine-related aspects, *EGUsphere*, pp 1–34, 2025. https://doi.org/10.5194/egusphere-2025-3708
[43] Kärcher, B. and Fabian, P. Dynamics of aircraft exhaust plumes in the jet-regime, *Ann. Geophys.*, 1994, **120**, (10), pp 911–919.
[44] Kärcher, B. A trajectory box model for aircraft exhaust plumes, *J. Geophys. Res.*, 1995, **100**, pp 18835–18844.
[45] Kärcher, B., Burkhardt, U., Bier, A., Bock, L. and Ford, I. The microphysical pathway to contrail formation, *J. Geophys. Res.*, 2015, **1200**, (15), pp 7893–7927. https://doi.org/10.1002/2015JD023491
[46] Bier, A., Unterstrasser, S. and Vancassel, X. Box model trajectory studies of contrail formation using a particle-based cloud microphysics scheme, *Atmos. Chem. Phys.*, 2022, **220**, (2), pp 823–845. https://doi.org/10.5194/acp-22-823-2022
[47] Zink, J., Unterstrasser, S. and Burkhardt, U. Contrail formation for aircraft with hydrogen combustion - part 1: a systematic microphysical investigation, *EGUsphere*, pp 1–27, 2025b. https://doi.org/10.5194/egusphere-2025-3704
[48] Petzold, A., Neis, P., Rütimann, M., Rohs, S., Berkes, F., Smit, H., Krämer, M., Spelten, N., Spichtinger, P., Nédélec, P. and Wahner, A. Ice-supersaturated air masses in the northern mid-latitudes from regular in situ observations by passenger aircraft: vertical distribution, seasonality and tropospheric fingerprint, *Atmos. Chem. Phys.*, 2020, **200**, (13), pp 8157–8179. https://doi.org/10.5194/acp-20-8157-2020
[49] Teoh, R., Schumann, U., Voigt, C., Schripp, T., Shapiro, M., Engberg, Z., Molloy, J., Koudis, G. and Stettler, M. Targeted use of sustainable aviation fuel to maximize climate benefits, *Environ. Sci. Technol.*, 2022, **560**, (23), pp 17246–17255. https://doi.org/10.1021/acs.est.2c05781
[50] Wittmann, T., Lück, S., Bode, C. and Friedrichs, J. Modelling the condensation phenomena within the radial turbine of a fuel cell turbocharger, *Int. J. Turbomach. Propul. Power*, 2021, **60**, (3). https://doi.org/10.3390/ijtpp6030023
[51] Jansen, J. and Heymsfield, A. Microphysics of aerodynamic contrail formation processes, *J. Atmos. Sci.*, 2015, **720**, (9), pp 3293–3308. https://doi.org/10.1175/JAS-D-14-0362.1
[52] Wölk, J. and Strey, R. Homogeneous nucleation of H2O and D2O in comparison: the isotope effect, *J. Phys. Chem. B*, 2001, **1050**, (47), pp 11683–11701. https://doi.org/10.1021/jp0115805
[53] Kärcher, B. and Yu, F. Role of aircraft soot emissions in contrail formation, *Geophys. Res. Lett.*, 2009, **36**, p L01804. https://doi.org/10.1029/2008GL036649

## Appendix

### *A.1 Numerical solution for microphysical simulations*

Our study focuses on the thermodynamic aspects of contrail formation. However, the mixing process deviates from thermodynamic theory due to the activation of solid particles within the plume into water droplets, which reduce the plume's WV content by condensation. To capture these effects, numerical simulations taking relevant microphysical processes into account are necessary. Therefore, we propose a possible implementation of the generalised mixing curve equations within a numerical microphysics model.

For numerical simulations that capture the evolution of plume mixing over time starting from the initial exhaust values, a formulation based on the temporal evolution of the physical quantities is required. This involves solving the temporal differential equations for specific humidity (Equation (20)) and

https://doi.org/10.1017/aer.2026.10185 Published online by Cambridge University Press

enthalpy (Equation (21)), which have to be extended to account for the effects of microphysical processes. Within each time step, the relevant microphysical processes that change the specific humidity are condensation of WV on particles and evaporation of water, while the temperature changes due to the latent heat of these processes. To efficiently solve these coupled equations, we propose an operator splitting method to separate the thermodynamic and microphysical processes. An explicit Euler approach is employed to calculate the specific humidity $q_\mathrm{i}$ and temperature $T_\mathrm{i}$ from their previous values

$$q_\mathrm{i} = q_{\mathrm{i}-1} + \Delta t\, \mathcal{D}_\mathrm{i}(q_\mathrm{a} - q_{\mathrm{i}-1}), \qquad \text{for i} \in [1, \mathrm{N_t}] \tag{A1}$$

$$T_\mathrm{i} = T_{\mathrm{i}-1} + \Delta t\, \mathcal{D}_\mathrm{i} \left( \frac{h_\mathrm{a}}{c_p(q_{\mathrm{i}-1}, T_{\mathrm{i}-1})} - T_{\mathrm{i}-1} \right), \quad \text{for i} \in [1, \mathrm{N_t}] \tag{A2}$$

where $\mathcal{D} = \dot{m}_\mathrm{mix}/m_\mathrm{mix}$ is called entrainment rate and defined by the ratio of temporal change in plume mass related to the current plume mass and $N_\mathrm{t}$ is the number of time steps of the numerical simulation. We assume that the initial state $(q_0, T_0)$ and ambient state $(q_\mathrm{a}, T_\mathrm{a})$ are either known or can be calculated from the given conditions. The numerical formulation for specific humidity (Equation (A1)) follows directly from Equation (20). However, the numerical equation for temperature (Equation (A2)) requires an additional assumption to be derived from the enthalpy Equation (21): for a numerical approach, the time step $\Delta t$ is small, leading to small changes in specific humidity and enthalpy. Consequently, the heat capacities $c_\mathrm{p}\ (q_\mathrm{i}, T_\mathrm{i})$ and $c_\mathrm{p}\ (q_{\mathrm{i}-1}, T_{\mathrm{i}-1})$ can be approximated as constant during one time step. This allows us to simplify the expression for the change in enthalpy: $h_\mathrm{i} - h_{\mathrm{i}-1} = \int_{T_{\mathrm{i}-1}}^{T_\mathrm{i}} c_p(q, \tilde{T})\, d\tilde{T} \approx c_p(q_{i-1}, T_{\mathrm{i}-1})\Delta T$. This simplification leads to the numerical formulation of the temperature (Equation (A2)).

To evaluate the microphysical processes, it is essential to calculate the relative humidity $\mathrm{RH_{w,i}}$ for each time step. This can be achieved by calculating the partial pressure $p_\mathrm{wv,i}$ from $q_\mathrm{i}$ using Equation (13). The resulting partial pressure can then be converted to relative humidity corresponding to the current temperature $T_\mathrm{i}$. To take microphysical processes into account, the amount of WV that evaporates or condenses, denoted as $\Delta q_\mathrm{i}$, is calculated. The effective amount of evaporation or condensation then alters the temperature via the latent heat $L_\mathrm{h,i}$, given by $\Delta T_\mathrm{i} = \frac{\Delta q_\mathrm{i} L_\mathrm{h,i}(T_\mathrm{i})}{c_\mathrm{p}(q_\mathrm{i}, T_\mathrm{i}) m_\mathrm{tot,i}}$. To ensure that the energy conservation is fulfilled during the mixing process, it is crucial that the parametrisations of the heat capacity and latent heat are consistent. For the operator splitting to be valid, the changes in specific humidity and temperature due to the microphysical processes should not exceed a certain, previously defined threshold. If the microphysical changes exceed this threshold, the time step needs to be reduced to maintain the validity of the operator splitting.

This algorithm is similar to the one described in Ref. [46]. The only changes result from the use of the differential equations for specific humidity and enthalpy instead of mass mixing ratio and temperature.

**Cite this article:** Hillenbrand D. and Unterstrasser S. Contrail formation: generalised theory and a mitigation proposition for fuel-cell-propelled aircraft. *The Aeronautical Journal*, https://doi.org/10.1017/aer.2026.10185